The Semiexperimental Approach at Work: Equilibrium Structure of Radical Species

The semi-experimental approach at work: Equilibrium structure of radical species

Silvia Alessandrini,*,† Mattia Melosso,† Luca Bizzocchi,† Vincenzo Barone,‡ and Cristina Puzzarini*,†

†*Dipartimento di Chimica "Giacomo Ciamician", Università di Bologna, Via F. Selmi 2, I-40126 Bologna, Italy*

‡*INSTM, via G. Giusti 9, 50121 Firenze, Italy*

E-mail: silvia.alessandrini7@unibo.it; cristina.puzzarini@unibo.it

Abstract

The so-called semi-experimental (SE) approach is a powerful technique for obtaining highly accurate equilibrium structures for isolated systems. This Featured Article describes its extension to open-shell species, thus providing the first systematic investigation on radical equilibrium geometries to be used for benchmarking purposes. The small yet significant database obtained demonstrates that there is no reduction in accuracy when moving from closed-shell species to radicals. We also provide an extension of the applicability of the SE approach to medium-/large-sized radicals by exploiting the so-called "Lego-brick" approach, which is based on the assumption that a molecular system can be seen as formed by smaller fragments for which the SE equilibrium structure is available. In this Featured Article we show that this model can be successfully applied also to open-shell species.

Introduction

Rotational spectroscopy is a high-resolution experimental technique that enables a detailed characterization of isolated species or small clusters. Rotational constants, the leading terms of this spectroscopy, are usually determined with an accuracy better than 1 part in 10^8. They are proportional to the inverse of the corresponding principal moment of inertia I_i (in frequency units):

$$B^i = \frac{\hbar}{4\pi I_i} \,, \tag{1}$$

where i refers to the principal inertial axis (a, b or c, these leading to $B^a = A$, $B^b = B$ or $B^c = C$, respectively, with $A \geq B \geq C$). In turn, the inertia tensor $\mathbf{I}$ is a function of the molecular structure:

$$\mathbf{I} = \sum_K M_K (R_K^2 \mathbf{1} - \mathbf{R}_K \mathbf{R}_K^T) \,, \tag{2}$$

where the sum runs over all nuclei. $\mathbf{R}_K$ is the vector collecting the coordinates of K-th nucleus and M_K is the corresponding atomic mass. The relationships 1 and 2 are such

that very small modifications in the geometrical parameters lead to sizeable changes in the rotational constants. To give an example, a distance of 1.1289 Å for CO corresponds to a rotational constant B of 57841.66 MHz; increasing such bond length by about 1 mÅ decreases B by 102.34 MHz.[1]

Within the rigid-rotor approximation, rotational constants are straightforwardly derived from the molecular structure. Unfortunately, the inverse problem is not as simple: already for triatomic molecules the number of geometrical parameters exceeds the number of rotational constants. An additional complication arises from the non-rigidity of any molecular species, which requires to account for vibrational effects. To address the first issue, different isotopic species sharing the same geometry are usually employed in order to increase the number of data to be used in the structural determination via a least-square fit.[2–6] To account for vibrational effects, it is necessary to introduce how rotational constants depend on vibration. According to second-order perturbation theory (VPT2),[7] we obtain:

$$B_v^i = B_e^i - \sum_r \alpha_r^i \left(\mathrm{v}_r + \frac{d_r}{2} \right) \ , \tag{3}$$

where α_r^i denotes the vibration-rotation interaction constants; the sum runs over all the r vibrational modes, d_r being their degeneracy. Focusing on the vibrational ground state, eq. 3 becomes

$$B_0^i = B_e^i + \Delta B_{\mathrm{vib}}^i = B_e^i - \frac{1}{2} \sum_r \alpha_r^i d_r \ . \tag{4}$$

As pointed out in the literature, the magnitude of the vibrational contribution, ΔB_{vib}, ranges from 0.1% to 0.7%, and in most cases –for semi-rigid molecules– is smaller than 0.5%.[1,4] Despite ΔB_{vib} being such a small correction, its impact on structural determinations is relevant. First of all, from a theoretical point of view and within the Born-Oppenheimer (BO) approximation,[8] different isotopologues have the same geometry only if this latter is the equilibrium one (r_e), which corresponds to the minimum of the potential energy surface (PES). From a practical point of view, neglecting vibrational corrections and, thus, using

the B_0 values in the structural determination leads to the so-called r_0 effective structure. Despite the difference between the ground-state I_0 and equilibrium I_e inertia moments is, in most cases, less than 1%, r_0 and r_e differ in a significant manner. Furthermore, since vibrational effects are isotopologue-dependent, r_0 results depend on the number and type of isotopic species considered.[9,10]

The first attempts to account for vibrational effects in the derivation of molecular structures date back to the 1950s, i.e., some decades before quantum chemistry became a reliable, accurate, and affordable tool for structural and spectroscopic studies. Based on the hypothesis that the $I_0 - I_e$ difference remains constant upon isotopic substitution, Costain introduced the so-called r_s substitution structure,[11] which is obtained by calculating the Cartesian coordinates of the atom isotopically substituted (when moving from one isotopic species to another) using Kraitchman's equations.[12] Despite still being used nowadays, limitations and flaws in r_s have been pointed out in the literature.[5,13] An enlightening example is provided by the molecular structure of monofluorodiacetylene (HC_4F). In ref. 14, it was shown that the r_s structure is not able to properly describe the changes in the –C≡C(–F) distance due to substitution of hydrogen by fluorine, i.e., when moving from diacetylene to HC_4F: the r_s distance results ∼20 mÅ longer than the equilibrium value. To improve the substitution method, the mass-dependence of I_0 was introduced,[15] thus leading to the definition of the so-called r_m mass-dependent structure. For this latter, two variants, namely $r_m(1)$ and $r_m(2)$, are available, with 1 and 2 indicating the number of additional parameters to be evaluated.[15] Among the methodologies that account for vibrational effects in a non-rigorous manner, the best approximation to r_e is offered by the r_m structure, with an agreement usually ranging in the 2-7 mÅ interval for bond lengths and 0.4-1° for angles.[16–18] However, the associated uncertainties tend to be often smaller than these differences.[16–18] Furthermore, in molecules containing hydrogen atoms, the structural parameters involving these latter are often not well reproduced.[4] To overcome this shortcoming, the so-called 'Laurie' correction can be introduced, which implies an additional parameter to be determined[19] without however the

guarantee of getting reliable results.[5,20]

To obtain equilibrium structures, it is necessary to know the equilibrium rotational constants for a sufficient number of isotopic species. According to eqs. 3 and 4, the B_e values can be obtained from the knowledge of the rotational constants for the vibrational ground state and all singly-excited vibrational states. In principle, such information can be retrieved from rotational and ro-vibrational spectroscopic studies. However, already for tetratomic molecules, the experimental derivation of the vibration-rotation interaction constants for all vibrational modes is a challenging task which, in practice, becomes an impossible one as soon as the molecule contains more than 4 atoms. To overcome such a limitation, Pulay et al.[3] proposed the quantum-chemical calculation of vibrational corrections and applied it to the derivation of the so-called semi-experimental (SE) equilibrium structure (r_e(SE)) of methane. The C−H equilibrium distance they obtained, 1.0862(5) Å,[3] employing vibrational corrections computed at the Hartree-Fock (HF) level, turned out to be very accurate and was later confirmed by a re-determination of 1.08595(30) Å, which used high-level coupled-cluster (CC) techniques for the required quantum-chemical calculations.[21] While the procedure for obtaining the r_e(SE) structure is detailed in the methodology section, it should be mentioned that Pawłowski and coworkers[22] demonstrated that the SE equilibrium bond lengths conservatively have an accuracy of about 1 mÅ provided that electron correlation is considered in the calculation of the vibration-rotation interaction constants. However, more recently, a benchmark study showed that even a global hybrid density functional like B3LYP[23,24] in conjunction with a double-zeta quality basis set provides vibrational corrections able to meet the 1 mÅ accuracy for bond lengths,[25] thus allowing the r_e(SE) determination for larger and larger systems.[26–28]

In the last two decades, owing to the software and hardware developments on the one side and new experimental techniques on the other (e.g., laser ablation of solid compounds[29]), the SE approach has established itself as the most powerful and reliable methodology for obtaining accurate equilibrium structures of isolated systems.[26–28,30–32] While an exhaustive

survey of the literature on SE equilibrium structures is beyond the scope of this paper, representative examples are provided by refs. 25–28,30–49. For closed-shell species, a comprehensive compilation of r_e(SE) geometries is offered by the so-called SE127 database,[45,50] which also collects the original references. Indeed, as demonstrated in ref. 22, it is able to derive very accurate structural parameters avoiding the shortcomings of pure experimental determinations mentioned above. For example, while the single computed α_r values might be affected by Coriolis coupling, their half-sum is devoid of any resonance.[5] Conversely, in the experimental derivation of vibration-rotation interaction constants, the vibrational state of interest might be affected by interactions with other states, thus leading to perturbed α values. If these perturbations are other than the Coriolis coupling mentioned above, then their effects do not cancel out when performing the sum of eq. 4.

Among isolated systems, radical species are probably the most challenging ones. From a pure theoretical point of view, for quantum-chemical methodologies based on a single Slater determinant (HF theory and post-HF methods), the reference wave function can be described using either the unrestricted (UHF) or the restricted open-shell (ROHF) formulation.[51] The former is usually preferred also for its ease of implementation. However, the UHF wave function is inevitably contaminated by higher electronic spin states, thus having the major drawback of being a not-exact eigenfunction of the total spin operator ($\boldsymbol{S}^2$).[51,52] In the case of strong spin contamination, one can resort to the ROHF wave function, which is an exact eigenfunction of $\boldsymbol{S}^2$, but is not free from limitations such as the impossibility to identify a unique set of canonical molecular orbitals.[51,53] The choice between UHF and ROHF formulations can affect the *ab-initio* equilibrium structure (r_e) of open-shell species.[54] Concerning density functional theory (DFT), Menon and Radom[55] suggested that, in unrestricted double-hybrid procedures, the opposite behavior of UHF and UMP2 (unrestricted Møller-Plesset second-order theory[56,57]) usually leads to reasonable results when the spin contamination is not too high. However, in the presence of non-negligible electron delocalization, this error compensation might become ineffective. While DFT energies are not used

in the present context, this problem might affect the accuracy of gradients and Hessians, especially when parallel- and opposite-spin MP2 contributions have different coefficients.[58] While vibrational corrections to rotational constants have been found negligibly affected, caution should be taken for equilibrium geometry evaluations.[59]

For open-shell species, accurate reference structures to be used for benchmarking different computational approaches have never been reported in the literature, at least in a systematic way. On the experimental side, radicals are unstable and reactive; thus, they are challenging species to be investigated and characterized. In this respect, quantum chemistry often plays a crucial role in providing accurate predictions and guidance in the interpretation of experiments.[60–64]

The aim of this work is (*i*) to systematically apply the SE approach to a significant set of small radical species ranging from diatomics to tetratomic systems, and (*ii*) to extend the potentialities of this methodology to the accurate prediction of equilibrium structures for large radicals. The first target will allow us to verify that there is no accuracy reduction in the SE approach when moving from closed-shell species to radicals. As a consequence, this will lead to the definition of a small database, which will be surely useful for future studies and will provide the first step toward a systematic characterization of open-shell species structures. For the second purpose, the so-called "Lego-brick" approach (see Methodology)[45,50,65,66] will be employed: its potentialities and limitations will be addressed. The organization of the manuscript reflects this double aim. In the next section, the methodological aspects of the SE and "Lego-brick" approaches are explained in some detail. Subsequently, results are presented and discussed: in the first part the SE database is addressed; in the second part, the outcomes of the "Lego-brick" approach are provided. In the Results section, we proceed in an increasing-the-complexity order, from diatomics to polyatomics, and we conclude with the prediction of accurate structures for large radicals. The outcomes of our work are summarized in the Concluding Remarks section.

Methodology

In this section, the methodology employed in this work together with the corresponding computational details are provided. The dataset considered for the benchmark of the r_e(SE) structures of radicals includes systems ranging from diatomics to tetratomic (planar) species. The complete list is reported in Table 1. The experimental rotational constants of each species have been collected from the literature, with the corresponding references being indicated in Table 1 for each isotopologue considered.

For medium- to large-sized radicals (i.e. containing more than 4-5 non-hydrogen atoms), experimental data are very limited, with the phenyl radical[33,67] being –to the best of our knowledge– a rather unique exception. Indeed, the number of medium-/large-sized radicals whose rotational spectrum has been investigated is quite small, and very rarely isotopic species other than the parent one have been studied. Therefore, for this type of radicals, we introduce a different strategy, which employs the SE results available for small radicals and exploits the "Lego-brick" approach to "extend" them to larger systems. The radicals here considered are phenyl (whose r_e(SE) is accurately known[67]), β-cyanovinyl (cis and trans[68]), β-trans-chlorovinyl (^{35}Cl isotopologue[69]), CH_2CHCO (s-trans-3-propenalyl and 3-propenolyl[70]), C_nS with $n = 4$, 6, and 8.[71] $C_{10}S$ and the naphthyl radical have instead been considered as good candidates for future studies. All these radicals are shown in Figures 1 and 2. Finally, the propargyl radical is considered as separate case study to address, within the "Lego-Brick" approach, the issue of resonance-stabilized open-shell systems.

The semi-experimental approach

As anticipated in the Introduction, the r_e(SE) structure is obtained by a least-squares (LSQ) fit of the molecular structural parameters to the SE equilibrium inertia moments I_e (or alternatively to the SE equilibrium rotational constants B_e) for a sufficiently large number of isotopologues of the considered molecular species (possibly accounting for substitution at

each atom). In all the cases here considered, the `xrefit` module of the CFOUR quantum-chemistry package[72,73] has been used for the LSQ fits.

According to eq. 1, the SE equilibrium inertia moments I_e are straightforwardly derived from the SE equilibrium rotational constants B_e. These latter are obtained from the rearrangement of eq. 4:

$$B_e^i(\mathrm{SE}) = B_0^i(\mathrm{exp}) - \Delta B_{\mathrm{vib}}^i(\mathrm{theo}) - \Delta B_{\mathrm{ele}}^i(\mathrm{theo}) \ , \tag{5}$$

where $B_0^i(\mathrm{exp})$ and $\Delta B_{\mathrm{vib}}^i(\mathrm{theo})$ denote the experimental ground-state rotational constants and the computed vibrational corrections, respectively. In the equation above, an additional term appears: $\Delta B_{\mathrm{ele}}^i(\mathrm{theo})$, which is the calculated electronic correction to rotational constants (see below). This contribution is a non-adiabatic term, thus it is usually by far smaller than the vibrational one and often negligible.[4,25] However, its impact on the SE equilibrium structure determination for radicals will be inspected in our study.

According to eq. 4, vibrational corrections require the computation of the vibration-rotation interaction constants. While the readers are referred to, for example, refs. 5,7,74 for their detailed expression within VPT2, here we recall that for their evaluation, in addition to moments of inertia and their derivatives, harmonic frequencies (in a normal coordinate representation), Coriolis constants and semi-diagonal cubic force constants are needed. For the computation of the vibration-rotation interaction constants, two different quantum-chemical programs have been employed in this study: CFOUR[72,73] and Gaussian16.[75] The former software has been used for MP2 and CC singles and doubles with a pertubative treatment of triples (CCSD(T))[76] calculations, while the latter has been employed for DFT computations. Both quantum-chemical programs compute the harmonic force field using analytical second-derivative techniques (in a normal coordinates representation) and the full set of cubic force constants by numerical differentiation. Noted is that for large molecules, the second and semi-diagonal third derivatives needed for the evaluation of vibrational corrections can be

obtained by a much cheaper approach employing analytical gradients.[77,78]

The $\Delta B_{\rm ele}$ electronic corrections to rotational constants are due to the contribution of electronic distribution to the moments of inertia and are thus connected to the rotational g-factor. While the reader is referred to, for example, refs. 2,79 for the underlying theory, the expression for their calculation is here reported:

$$\Delta B^i_{\rm ele} = \frac{m_e}{m_p}\, g^i\, B^i_e\,, \tag{6}$$

where m_e and m_p are the mass of the electron and proton, respectively, and g^i denotes the diagonal element of the rotational g-factor tensor along the i inertial axis, which is computed as the second derivative of the energy with respect to magnetic field using gauge-invariant atomic orbitals.[80] Electronic corrections have been computed at the HF level (using the unrestricted formulation) in combination with the aug-cc-pVTZ basis set.[81–83]

In the determination of the r_e(SE) structure, it should be recalled that, for planar species, only two rotational constants are independent because of the following relationship:

$$\frac{1}{C_e} = \frac{1}{A_e} + \frac{1}{B_e}\,. \tag{7}$$

While a redundant (linearly dependent) set of data can in principle be used, this might affect the stability and the accuracy of the LSQ procedure. Therefore, among the three possible combinations, the most suitable one needs to be selected. To guide this choice, the first derivative of the rotational constants with respect to the structural parameters can be inspected, thus leading to the selection of the two rotational constants showing the largest dependence.[141] In those cases where all rotational constants provide significant information, the combination of the two data to be used in the fit was based on their relative experimental accuracy and not on the expected accuracy of the vibrational corrections as done in previous works.[22] To give an example, in the case of the NH_2 radical, A_0 is very well determined with an error of 0.01 MHz for a value of 710302.019 MHz and B_0 and C_0, which

Table 1: Summary of the radicals[a] considered for the benchmark dataset together with the isotopic species used in the r_e(SE) determination.

Radical	Isotopic sp. and reference	Radical	Isotopic sp. and reference
	DIATOMICS		
Methylidyne $^2\Pi_r$	CH [84]	Boron monoxide $^2\Sigma^+$	BO [85]
	^{13}CH [86]		^{11}BO [85]
Hydroxyl $^2\Pi_i$	OH [87]	Nitrogen monoxide $^2\Pi_r$	NO [88]
	OD [89]		^{15}NO [90]
	^{17}OH [91]		N^{17}O [92]
	^{18}OH [93]		N^{18}O [88]
Sulfanyl $^2\Pi_i$	SH [87]		^{15}N^{18}O [92]
	SD [94]	Sulfur Monoxide $^3\Sigma^-$	SO [95]
Imidogen $^3\Sigma^-$	NH [96]		^{33}SO [97]
	ND [98]		^{34}SO [95]
	^{15}NH [99]		^{36}SO [97]
	^{15}ND [100]		S^{17}O [95]
Phosphinidene $^3\Sigma^-$	PH [101]		S^{18}O [95]
	PD [102]	Nitrogen Sulfide $^2\Pi_r$	NS [103]
Arsinidene $^3\Sigma^-$	AsH [104]		N^{33}S [105]
	AsD [104]		N^{34}S [105]
Cyanogen $^2\Sigma$	CN [106]		^{15}NS [105]
	C^{15}N [107]		
	^{13}CN [108]		
	^{13}C^{15}N [109]		
	TRIATOMICS		
Methylene $^3B_1$	CH_2 [110]	Silicon hydroxide $^2A'$	SiOH [111]
	CHD [112]		^{30}SiOH [111]
Amidogen $^2B_1$	NH_2 [113]		SiOD [111]
	NHD [114]		Si^{18}OH [111]
	$^{15}NH_2$ [115]	Thioformyl $^2A'$	HCS [116]
	^{15}NHD [117]		DCS [116]
	ND_2 [118]		H^{13}CS [119]
	$^{15}ND_2$ [120]	Thiohydroxymethylidyne $^2A'$	HSC [121]
Phosphidogen $^2B_1$	PH_2 [122]		DSC [121]
	PHD [123]		HS^{13}C [119]
	PD_2 [124]	Sulfoxyl radical $^2A''$	H^{32}S^{16}O [125]
Arsenic hydride $^2B_1$	AsH_2 [126]		D^{32}S^{16}O [127]
	AsD_2 [128]	Thioethenylidene $^3\Sigma^-$	CC^{32}S [129]
Formyl ; $^2A'$	HCO [130]		CC^{34}S [131]
	DCO [132]		^{13}CC^{32}S [133]
			C^{13}C^{32}S [133]
			^{13}C^{13}C^{32}S [133]
	TETRATOMICS		
Fluoroformyloxyl $^2B_2$	FCO_2 [134]	Hydridotrioxygen $^2A''$	HO_3 [135]
	FCO^{18}O [136]		DO_3 [135]
	FC$^{18}O_2$ [137]		H^{18}OOO [36]
Chloromethyl radical $^2B_1$	$^{35}ClCH_2$ [138]		HO^{18}OO [139]
	$^{37}ClCH_2$ [138]		HOO^{18}O [139]
cis-Carboxyl $^2A'$	HOCO [140]		HO^{18}O^{18}O [36]
	DOCO [140]		H^{18}O^{18}O^{18}O [36]
	H^{18}OCO [140]		D^{18}OOO [139]
	HOC^{18}O [140]		DO^{18}O^{18}O [139]
	HO^{13}CO [140]		D^{18}O^{18}O^{18}O [139]
trans-Carboxyl $^2A'$	HOCO [140]	cis-Hydroxidooxidosulfur $^2A''$	HOSO [37]
	DOCO [140]		DOSO [37]
	H^{18}OCO [140]		HO^{34}SO [37]
	HOC^{18}O [140]		H^{18}OS^{18}O [37]
	HO^{13}CO [140]		

[a] The experimental rotational constants are taken from the indicated references.

are 388289.458 MHz and 245013.520 MHz, respectively are affected by a similar uncertainty (0.015 MHZ and 0.011 MHz);[113] thus, the smallest relative errors are noted for A_0 and B_0, and their combination has been employed in the LSQ fit. However, in view of the large set of isotopologues available, NH_2 will be employed as a sort of case study to test the different combinations of rotational constants in the LSQ fit, also considering the use of all of them at the same time (redundant set of data). For the PH_2 radical, the situation is similar[122] and the A_0/B_0 pair has been used. Differently, for the AsH_2 species, the smallest relative errors are observed for B_0 and C_0,[126] and therefore their combination has been chosen. Particular cases are diatomic and linear molecules, which have only two non-vanishing and identical rotational constants. In this case, for each isotopologue, only one rotational constant has to be considered in the fitting procedure.

The "Lego-brick" approach for radicals

As mentioned in the introductory part of the Methodology section, for medium- to large-sized radicals, the SE approach is exploited in the framework of the "Lego-brick" scheme, with the focus somewhat shifting from benchmarking to prediction of structure and rotational constants. From a computational point of view, the accurate determination of their equilibrium structures is hampered by the computational cost and the intrinsic complexity of describing an open-shell electronic configuration (see Introduction). Prompted by the excellent results obtained for small PAHs,[66,142] benzene-derivatives,[143] and long chains,[129] the present work introduces a protocol for the accurate yet cost-effective determination of the equilibrium geometry of radical species. As already stated, this is based on the so-called "Lego-brick" approach,[65,66] which in turn exploits the template-molecule (TM) approach[25] combined with the linear-regression (LR) approach.[50]

According to the TM model, a medium-/large-sized molecular system can be seen as the combination of smaller molecular fragments, for which accurate equilibrium structures are available. In the TM scheme, the first step is to obtain the equilibrium geometry for

the target molecule at an affordable computational cost (thus using DFT methodologies, $r_e^{\mathrm{DFT,T}}$). This is then improved by incorporating the corrections for the molecular fragments ($\Delta r_e^{(\mathrm{F})}$):

$$r_e^{\mathrm{TM,T}} = r_e^{\mathrm{DFT,T}} + \Delta r_e^{(\mathrm{F})} \,, \tag{8}$$

with r denoting a generic structural parameter and $\Delta r_e^{(\mathrm{F})}$ being

$$\Delta r_e^{(\mathrm{F})} = r_e^{\mathrm{SE,F}} - r_e^{\mathrm{DFT,F}} \,, \tag{9}$$

and F denoting the fragment and $r_e^{\mathrm{SE,F}}$ the r_e(SE) structure of the fragment.

If, in the target molecule, there are structural parameters (bonds) connecting the envisaged fragments, then these need to be corrected in order to improve the original accuracy of DFT methodology employed for $r_e^{\mathrm{DFT,T}}$. To do so, the LR approach is used:

$$r_e^{\mathrm{LR,T}} = (1 + a) \times r_e^{\mathrm{DFT,T}} + b \,, \tag{10}$$

where a and b are the linear regression parameters, which depend on the DFT level chosen and have been taken from ref. 50. In the present study, based on previous work,[66,129,143] for $r_e^{\mathrm{DFT,T}}$, we have employed the double-hybrid rev-DSDPBEP86-D3BJ[58] functional in conjunction with the jun-cc-pV(T+d)Z[81,83,144,145] basis set, where "+d" refers to third-period elements and "D3BJ" indicates the incorporation of empirical dispersion corrections.[146,147] Hereafter, this level of theory is shortly denoted as revDSD/junTZ.

While the "Lego-Brick" approach is well tested for closed-shell species, this is the first application to radicals. Two different strategies have been tested. The first one, denoted as "parent_molecule–radical TM" approach, uses only one fragment for the TM approach, which is the "parent molecule" of the open-shell species, i.e., the closed-shell system obtained by adding a H atom on the radical site. As shown in Figure 1, the test cases selected for this first approach are the pairs benzene/phenyl radical, acrylonitrile/β-cyanovinyl radical (both

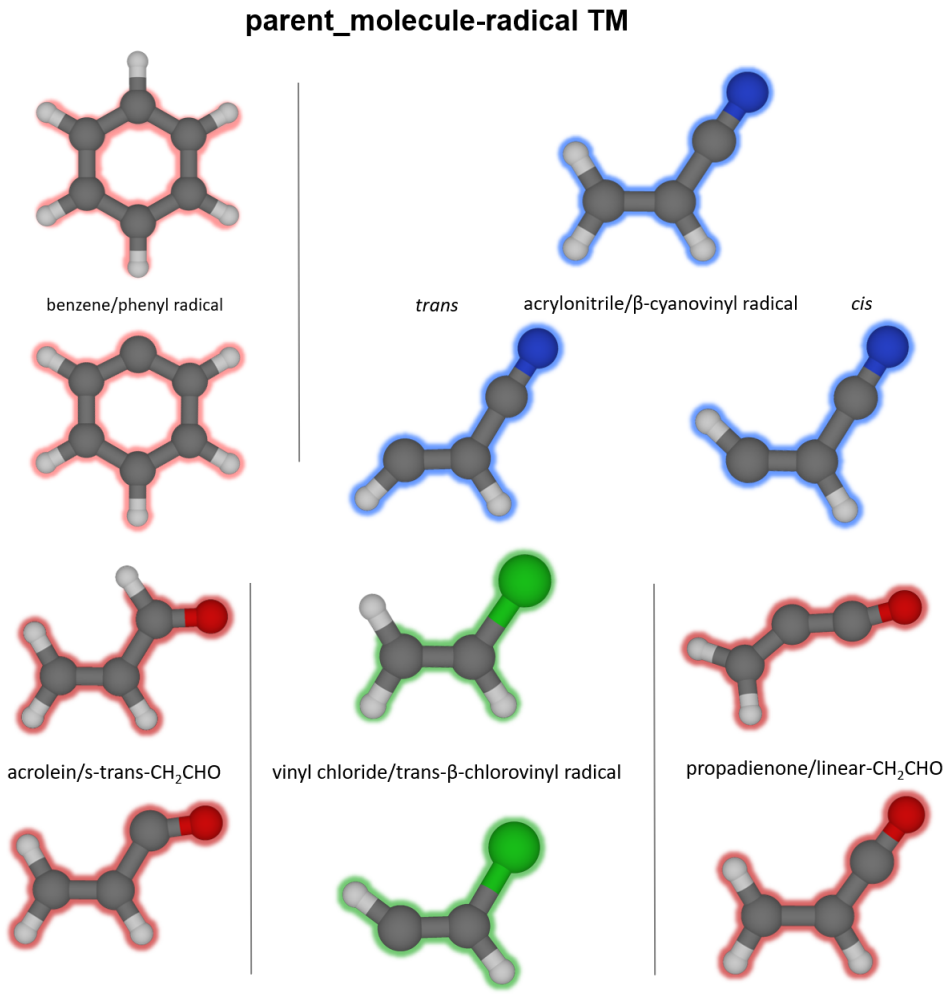

Figure 1: Test-case systems for the "parent_molecule–radical TM" approach: in each panel, the parent (top) and the radical species (bottom) are shown.

cis and trans), vinylchloride/chlorovinyl radical, acrolein/s-trans-CH_2CHCO radical, and propadienone/3-propendyl (also denoted as linear-CH_2CHCO), with the latter pair being the only case where one H atom is added (instead of removed) when moving to the radical species. Instead, the second strategy, denoted as "radical–radical TM" approach, employs more than one fragment: it combines closed-shell species with one radical fragment. This approach is illustrated in Figure 2, where the test cases considered are shown: the members of the C_nS family, with n = 4, 6, 8, and 10, the CH_2CHCO radicals (both the isomers previously mentioned), and the naphthyl radical. While for the C_nS (with the exception of n=10) and CH_2CHCO families experimental data are available, the naphthyl radical and

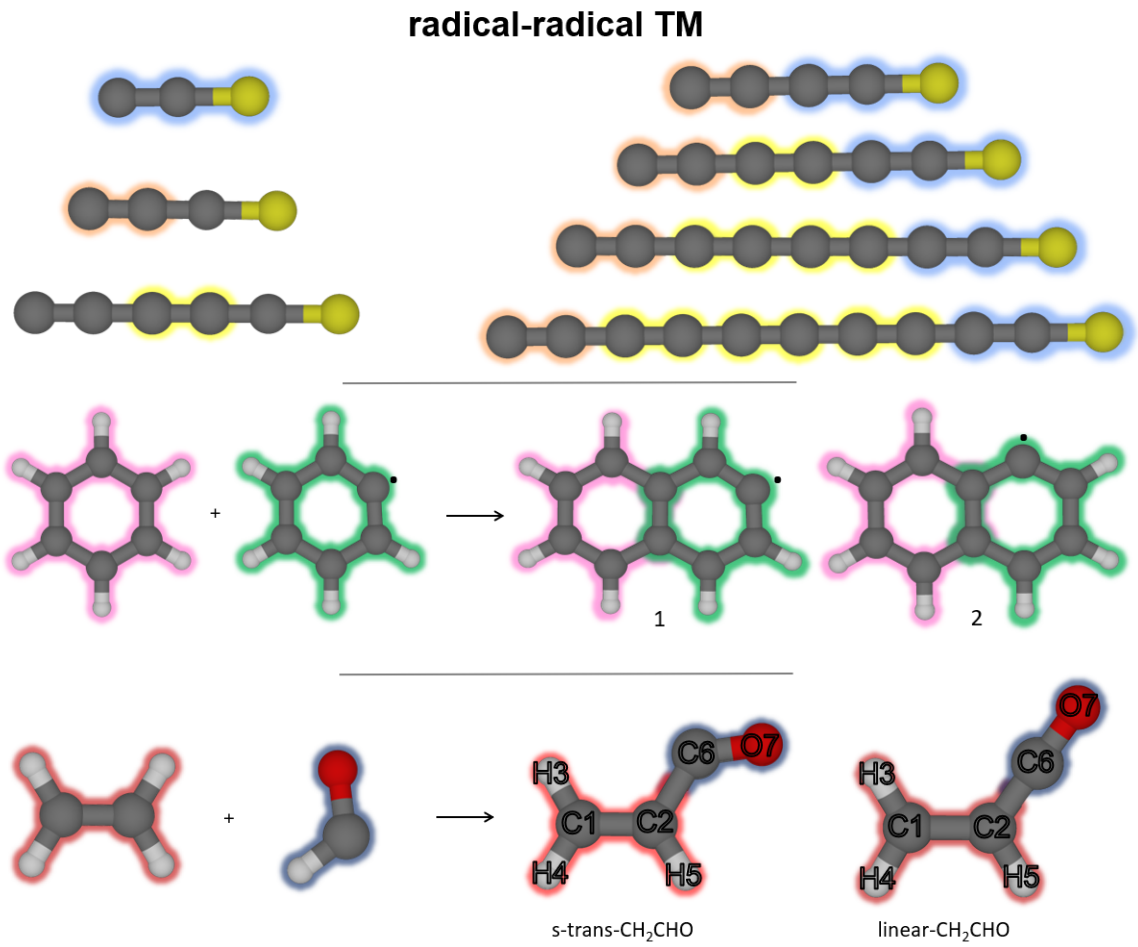

Figure 2: Test-case systems for the "radical–radical TM" approach: in each panel, the TM fragments (left) and the radicals (right) are shown. Colored halos are used identify to highlight the fragments within the raical species.

$C_{10}S$ are prospective ones. Based on the results obtained using the "radical–radical TM" approach (see next section), we indeed report the first accurate estimates of the equilibrium geometry and vibrational ground-state rotational constants for $C_{10}S$ and for both forms of the naphthyl radical shown in Figure 2 (1- and 2-naphthyl radicals). For both strategies, the results are assessed by comparing the equilibrium rotational constants obtained from the "Lego brick" approach with the experimental ones. To have a meaningful comparison, the former parameters have been augmented by vibrational corrections (the level of theory is detailed in the discussion). To apply the "Lego-brick" approach, the r_e(SE) structures of the closed-shell fragments were taken from the literature: ref. 50 (SE127 database) for benzene,

ethene, propadienone, acrolein, and acrylonitrile; ref. 148 for vinylchloride; ref. 149 for C_3S. Only for C_5S, the r_e(SE) structure was not available and, therefore, has been purposely derived in this work. Concerning the radical fragments, their r_e(SE) parameters have been derived in this work, with the only exception of the phenyl radical whose data come from ref. 33.

Results and Discussion

The results will be illustrated according to the organization of the Methodology section. First of all, the small benchmark of the SE approach applied to radicals will be presented, with the discussion being based on the system dimension: first diatomics, then triatomics, to conclude with planar tetratomic radicals. For all these species, we report the r_0 structure, which is obtained from the LSQ fit of the experimental B_0 values without any correction, the r_e(SE) structure, which considers vibrational corrections to experimental B_0 constants, and the SE equilibrium structure denoted as $r_e(\mathrm{SE})_{full}$, which is derived by incorporating both the vibrational and electronic corrections (see eq. 5). The standard deviations of the LSQ fits are collected in the Supporting Information (SI; Table S1). Subsequently, the results from the "Lego-brick" approach will be presented. In this case, as mentioned in the Methodology section, the accuracy of the resulting equilibrium geometries is discussed in terms of rotational constants and their comparison with the available experimental data.

Semi-experimental equilibrium structure dataset

Before proceeding with the detailed discussion of the results as outlined above, we present the outcome of the tests performed in order to investigate the level of theory used to compute vibrational corrections. For a selection of radicals for which the corresponding experimental values are available, the vibrational corrections have been calculated using the CCSD(T) method, within the frozen-core (fc) approximation, the double-hybrid B2PLYP functional

Table 2: Computed and experimental vibrational corrections to the rotational constants ($\Delta B^i_{\rm vib}$). All values in MHz.

Species	Rot. Const.	Exp.	CC/TZ[a]	B2/TZ[b]	revDSD/TZ[c]
SO	B	-86.20[150]	-81.60	-85.45	-79.90
BO	B	-248.74[151]	-232.79	-247.30	-240.38
CH	B	-8006.89[152]	-8011.18	-7696.93	-7592.56
OH	B	-10656.98[87]	-10768.88	-10534.53	-10391.58
SH	B	-4174.23[87]	-4163.85	-4060.51	-4001.63
NO	B	-263.38[88]	-104.14	-257.59	-180.31
NS	B	-94.20[105]	-103.12	-94.17	-101.75
HCO	A	6040.82[153]	5005.98	6434.49	8861.54
	B	-67.15[153]	-79.35	-98.28	-103.94
	C	-324.07[153]	-304.94	-301.76	-298.35
NH_2	A	8730.16[113,154]	3982.57	5668.88	6399.76
	B	-1617.93[113,154]	-1416.06	-1539.45	-1571.55
	C	-6248.66[113,154]	-6399.71	-6069.33	-5991.52
%MAE			14.9%	8.8%	15.8%
%MAE[d]			11.1%	9.3%	14.5%

[a] CC/TZ stands for fc-CCSD(T)/cc-pVTZ. [b] B2/TZ stands for UB2PLYP/cc-pVTZ. [c] revDSD/TZ stands for revDSD/junTZ. [d] Calculated without the contribution of the NO radical.

(in the unrestricted formulation: UB2PLYP),[155] both in conjunction with the cc-pVTZ basis set,[81,83] and the revDSD/junTZ level. The comparison is reported in Table 2, where the relative mean absolute errors (%MAEs) are also given. It is noted that, if the NO radical is excluded from the statistics, the three levels of theory provide similar %MAEs. Indeed, for NO, UB2PLYP leads to a very good agreement with experiment (2.2%), while the CCSD(T) value is nearly half of the experimental datum and revDSD/junTZ gives a result which is somewhat in between. Another outlier for CCSD(T) is the vibrational correction to A for NH_2. As noted in ref. 156, where a $\Delta B^A_{\rm vib}$ value of 5592.9 MHz was obtained at the CCSD(T)/aug-cc-pCVQZ level correlating all electrons, this discrepancy with respect to experiment is mainly ascribable to α^A_2. Indeed, this vibration-rotation interaction constant has a large experimental value (-68195.5 MHz) which is due to the fact that the bending motion is a large amplitude motion, thus not appropriately described by VPT2. Furthermore,

it is affected by a low-lying linear electronic excited state. If we exclude this datum, the %MAE for CCSD(T) reduces to 7.2%.

The overall conclusion that can be drawn from Table 2 is that all levels of theory provides vibrational corrections to rotational constants with an accuracy which is suitable for r_e(SE) determinations.[1,22] Indeed, errors of 20% on the vibrational corrections are estimated to lead uncertainties no larger than 0.1% on rotational constants.[1] Interestingly, revDSD/junTZ and, especially, UB2PLYP/cc-pVTZ perform well also in the case of radical species. This is an important outcome when, for example, reliable estimates for the vibrational ground-state rotational constants of a medium-sized open-shell molecule are needed to guide spectral recording and/or to support spectral analysis. In the following, however, since the systems considered range from to 2 to 4 atoms and since the aim is to obtain a benchmark dataset, the fc-CCSD(T)/cc-pVTZ level has been employed. This has been indeed considered as the level of reference in several benchmark studies.[22,25] The only exceptions are the NO radical because of the discrepancy noted above and the CN radical because of its well-known multireference character, which would require to incorporate up to quadruple excitations in the CC expansion.

Diatomic species

For diatomic radicals, the comparison between the r_0, r_e(SE) and $r_e(\mathrm{SE})_{full}$ structures is reported in Table 3, where the available literature values, mainly based on experimental data, are also given. It is first of all noted that the r_0 structures are well determined with the associated uncertainties being smaller than 1 mÅ, except for PH and AsH, whose bond lengths show an error of 1 mÅ. Due to asymptotic limits, in the presence of a single energy minimum, the r_0 bond distance, which describes the structure of the molecule in the vibrational ground state, is greater than its equilibrium counterpart.

Moving from r_0 to r_e(SE), the statistical error of the LSQ fit reduces, in most cases, by one order of magnitude. This is also associated with changes in the resulting bond lengths,

Table 3: Diatomic radicals: r_0, r_e(SE) (SE equilibrium structure incorporating vibrational corrections) and $r_e(\mathrm{SE})_{full}$ (SE equilibrium structure incorporating both vibrational and electronic corrections) results compared with literature data.

Species	r_0	r_e(SE)[a]	$r_e(\mathrm{SE})_{full}$[b]	r_e Literature
NH	1.0448(7)	1.0367(1)	1.03631(4)	1.03606721(13)[c] [100]
				1.037286 [157]
PH	1.430(1)	1.4220(1)	1.42166(6)	1.4222 [158]
AsH	1.531(1)	1.5231(2)	1.5241(5)	1.522370(86) [104]
SO	1.48399(2)	1.481233(2)	1.481163(1)	-
BO	1.20740(3)	1.20473(3)	1.204689(2)	1.20466[d]
CN	1.17441(3)	1.17228(2)	1.17211(2)	1.171800(6) [109]
				1.1717597(14)[c] [159]
CH	1.13026(2)	1.119791(4)	1.1180824(4)	1.11810[e] [160]
				1.119913 [157]
SH	1.3482(8)	1.34056(4)	1.34046(2)	1.3406194(3) [87]
OH	0.9778(7)	0.96988(9)	0.9708(2)	0.969616(9) [87]
				0.969789 [157]
NS	1.49705(1)	1.493759(4)	1.493660(5)	1.49403(4) [161]
NO	1.15369(2)	1.15254(1)	1.150871(6)	1.1506921(16) [90]

[a] Vibrational corrections at the fc-CCSD(T)/cc-pVTZ level of theory, except for CN and NO. For them, UB2PLYP/cc-pVTZ has been employed. See text.

[b] Electronic corrections (rotational g-tensor) at the HF/aug-cc-pVTZ level of theory.

[c] From an isotopic invariant fit. See refs. 100,159 for details.

[d] Pure theoretical result obtained by means of a CC-based composite scheme incorporating up to quadruple excitations and extrapolation to the complete basis set limit. [162]

[e] Pure theoretical result obtained by exploiting an extended HEAT protocol. [163]

which vary from 0.8 mÅ, in the case of NH, up to 10 mÅ, for the CH radical, with an average shortening of 5 mÅ. The incorporation of the electronic contribution in the LSQ fit (thus leading to the $r_e(\mathrm{SE})_{full}$) does not provide any significant modification (with only a couple of exceptions; *vide infra*), but in all cases it improves the associated errors.

For NH, CH and OH, the r_e(SE) value can be compared with the results from ref. 157, where the effects of fourth-order vibrational perturbation theory (VPT4) on the SE equilibrium structure were considered. According to that work, the CH bond distance is 1.119913 Å, which is thus in very good agreement with our r_e(SE) value of 1.119791(4) Å and deviates by about 2 mÅ from the other literature value of 1.11810 Å [160] reported in Table 3, which is

a pure, extremely accurate, computed result.[160,163] Such a difference vanishes once we move from r_e(SE) to $r_e(\mathrm{SE})_{full}$. Indeed, as in the case of $r_e(\mathrm{SE})_{full}$, the bond length from ref. 160 incorporates electronic effects in the equilibrium structure determination. Therefore, the present work confirms, for CH, the importance of incorporating electronic corrections in order to get an equilibrium distance fulfilling the 1-mÅ accuracy. This might be explained by the presence of a low-lying excited state. In such a case, it is also a matter of reliability because the differences between r_e(SE) and $r_e(\mathrm{SE})_{full}$ are larger than the associated statistical uncertainties. In passing we note the extremely too long bond length (1.137 Å) derived in ref. 164; in this respect, our $r_e(\mathrm{SE})_{full}$ value together with that of ref. 160 provide a solid benchmark result that can guide the selection of the level of theory to be employed in the characterization of radical species. For NH, our r_e(SE) value of 1.03631(4) Å is in good agreement with that reported in the literature by Melosso et al.[100] (1.03606721(13) Å), while both values are ∼1 mÅ shorter than that derived using the VPT4 contribution, this being 1.037286 Å.[157] The discrepancy reduces to about 0.5 mÅ if $r_e(\mathrm{SE})_{full}$ is considered. For the OH radical, our best estimate is 0.96988(9) Å and the value obtained using VPT4 is 0.969789 Å; thus, the difference is only ∼0.1 mÅ. This is also in good agreement with the experimental bond distance (from an isotopically invariant Dunham fit) obtained in ref. 87, which is underestimated by only 0.2-0.3 mÅ. Incorporation of the electronic correction increases the distance by 1 mÅ, thus in a non-negligible way but still within the intrinsic accuracy of the SE equilibrium structures.

Focusing on the other radicals, the largest deviation from the available literature value is observed for the NO radical. Indeed, for this species, our LSQ fit leads to an equilibrium bond distance of 1.15254(1) Å, while in ref. 90 an experimental value of 1.1506921(16) Å was obtained from an isotopically independent Dunham fit, this latter distance being about 2 mÅ shorter than our evaluation. This discrepancy might be related to the different set of isotopic species employed in the LSQ fit. However, it has to be noted that the difference is reduced to about 0.2 mÅ once the electronic correction is taken into account, the $r_e(\mathrm{SE})_{full}$

value being 1.150871(6) Å. This was somewhat expected because the experimental result of ref. 90 incorporates the effects of the breakdown of the BO approximation.

To summarize, for diatomics, the exploitation of the SE approach together with the availability of the rotational constants for at least two different isotopic species allows for obtaining equilibrium bond distances with an accuracy of 1 mÅ or even better. Our results point out the need of incorporating electronic corrections in order to meet such an accuracy whenever non-adiabatic effects cannot be neglected, this often being related to low-lying excited states.

Triatomic species

In Figures 3 and 4, the triatomic radicals considered in this study are shown and the results obtained (r_0, r_e(SE) and $r_e(\mathrm{SE})_{full}$ structures) are there compared. Figure 3 collects the triatomic S-containing radicals investigated in this work together with a couple of isovalent species. Figure 4 instead reports four XH_2 radicals having C_{2v} symmetry. The presentation of the results is based on the classification provided by these two figures.

Figure 3. The discussion of Figure 3 starts with the two radicals in the left panels: HCS (top) and HSC (bottom). Both of them are species of astrochemical relevance and their astronomical detection provided new insights into the interstellar sulfur chemistry puzzle.[165] As noted in Table 1, for both radicals, the isotopologues experimentally investigated are the main, the deuterated and the ^{13}C-containing species. However, for HCS and H^{13}CS, only $B_0 + C_0$ could be determined.

For HCS, starting from ∠HCS, its r_0 value of 131.9(1)° differs by about 1° from that previously determined,[116] which is 132.8(3)°. The ∠HCS angle then increases to 133.5°, i.e., by about 1.6°, when moving to the r_e(SE) and $r_e(\mathrm{SE})_{full}$ structures. Such a large $r_0 - r_e$ difference might be related to the experimental spectroscopic analysis;[116,119] indeed, for the main and ^{13}C-bearing species, only $B_0 + C_0$ could be determined and the $B_0 - C_0$ difference was

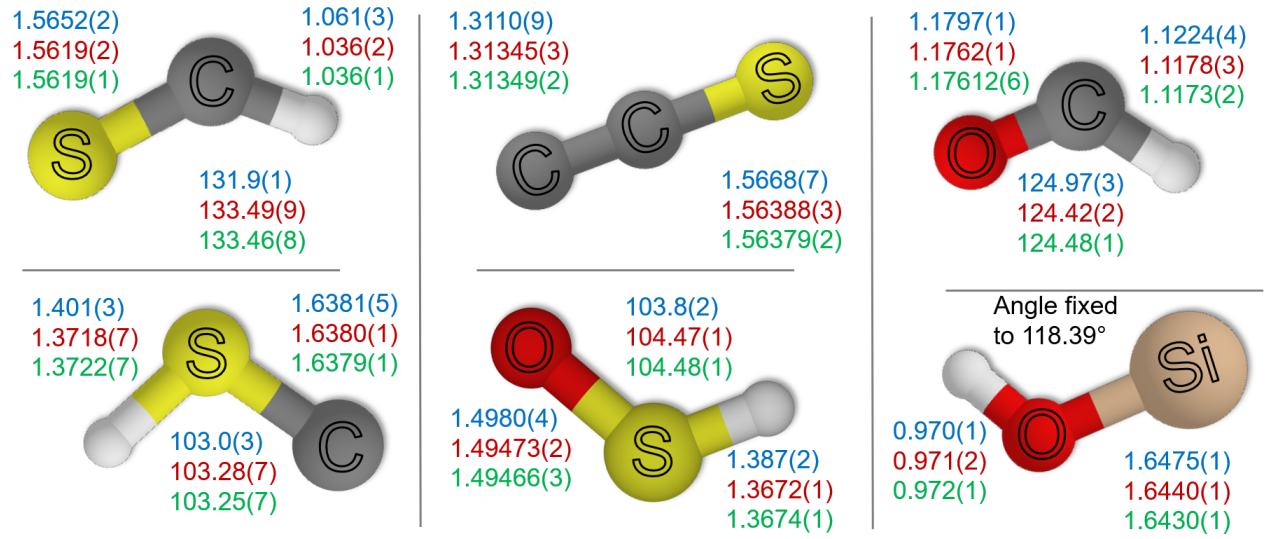

Figure 3: S-containing radicals and isovalent species: r_0 (light blue), r_e(SE) (red), and $r_e(\mathrm{SE})_{full}$ (green) structures. Bond lengths are in Å, angles in degrees.

kept fixed at the value derived from the r_0 value calculated in ref. 116 using the three rotational constants of DCS and B_0+C_0 for HCS. However, our resulting $r_e(\mathrm{SE})/r_e(\mathrm{SE})_{full}$ value of 133.5° overestimates by about 1° the accurate quantum-chemical derivation of 132.5°.[166] This latter is expected to have an accuracy of about a few tenths of degree, the level of theory employed being a composite scheme rooted in CCSD(T) which accounts for extrapolation to the complete basis set (CBS) limit and core-valence (CV) correlation effects (hereafter CCSD(T)/CBS+CV). As a sort of confirmation that the limitations noted above are related to the available spectroscopic parameters, such a large variation when moving from r_0 to r_e is not noted for HSC, whose r_0 angle is 103.0(3)° and becomes 103.28(7)° when applying the SE approach. This latter value is also in good agreement with the CCSD(T)/CBS+CV r_e counterpart of 103.1°,[166] while the experimental r_z* one of 104.2(2)°, obtained in ref. 121, results overestimated by about 1°.

For HCS, the considerations made above also apply to bond lengths. The r_0 value of C−S is 1.5652 Å, which becomes 1.5619 Å at the equilibrium, thus shortening by about 3 mÅ. This

*r_z is based on the average nuclear positions at 0 K and can be related to the substitution r_s structure.[167] For the specific details on HSC, the reader is refereed to ref. 121.

is still 7 mÅ longer than the corresponding CCSD(T)/CBS+CV value (1.555 Å).[166] These values agree with those previously reported in the literature, but the same does not apply to the H−C bond distance. Its r_0 value is 1.061(3) Å, which becomes 25 mÅ shorter (1.036 Å) when r_e(SE) and $r_e(\mathrm{SE})_{full}$ are considered; however, such a short value is not predicted by any theoretical method. Indeed, at the CCSD(T)/CBS+CV level, the H−C distance is 1.085 Å, thus ∼50 mÅ longer than the $r_e(\mathrm{SE})/r_e(\mathrm{SE})_{full}$ value. Once again, this result is surely the outcome of the experimental constraints mentioned above. Therefore, our conclusion is that additional experimental measurements on HCS are required to derive a complete, accurate and reliable, SE equilibrium structure for this radical. HCS thus provides a significant example of how the SE approach can be used to verify the reliability of experimental data once the latter do not result from a complete characterization. Different is the situation for HSC. For the S−C bond, the difference between r_0 and r_e is negligible, i.e. within 0.2 mÅ. Furthermore, the $r_e(\mathrm{SE})/r_e(\mathrm{SE})_{full}$ value of 1.638 Å well agrees with the CCSD(T)/CBS+CV result of 1.637 Å.[166] As expected, the H−S distance changes considerably when moving from r_0 to r_e: it shortens by about 30 mÅ. However, our $r_e(\mathrm{SE})/r_e(\mathrm{SE})_{full}$ value (1.372 Å) is still 8 mÅ longer than the CCSD(T)/CBS+CV result,[166] but still in better agreement than the experimental estimate of r_e, based on r_z, from ref. 121, which is 1.379(3) Å.

Two other S-bearing radicals have been investigated, which are depicted in the middle panels of Figure 3: the linear CCS species (top) and HSO (bottom). In analogy to the radicals previously discussed, both of them are species of astrochemical interest, which have been detected in the interstellar medium (ISM). Concerning CCS, the r_0 values of the C−C and C−S bond lengths are 1.3110(9) and 1.5668(7) Å, respectively. These become about 2 mÅ longer and 3 mÅ shorter, respectively, when moving to r_e(SE), with the associated errors decreasing by about one order of magnitude. This suggests that without accounting for vibrational effects the overall length of the radical is well determined, but the contributions of the two bonds are less accurate. Inclusion of electronic contributions leads to negligible modifications: ∼0.1 mÅ on C−S and 0.04 mÅ on C−C. The $r_e(\mathrm{SE})_{full}$ parameters result to

be: C−S 1.56379(2) Å and C−C 1.31349(2) Å. These bond lengths are very accurate because data for five isotopologues and isotopic substitution for each atom are available. Therefore, CCS is a good example for demonstrating that there is no reduction in accuracy when moving from closed-shell species to radicals in the application of the SE approach. The reliability of the r_e(SE)/r_e(SE)$_{full}$ structures is supported by the agreement well within 1 mÅ with a high-level quantum-chemical equilibrium geometry obtained at the CCSD(T)/CBS+CV level augmented for the contribution of full treatment of triple (fT) and quadruple (fQ) excitations (hereafter denoted as CCSD(T)/CBS+CV+fT+fQ) in ref. 168. Indeed, the latter structural parameters are 1.5624 Å for C−C and 1.3132 Å for C−S, which are expected to have an accuracy better than 1 mÅ.[1,5]

Focusing on HSO, it should be mentioned that this radical has only very recently been detected in the ISM[169] despite the fact that its first spectroscopic characterization dates back to 1981. This radical is bent and the r_0 structural parameters are: S−H = 1.387(2) Å, S−O = 1.4980(4) Å, and ∠HSO = 103.8(2)°. The two bond lengths shorten to 1.3672(1) Å and 1.49473(2) Å, respectively, when moving to the r_e(SE) geometry, while the angle increases to 104.47(1)°. As expected, since the rotational spectrum has been measured only for the parent and deuterated species and in view of the large mass change in the H/D substitution, relevant vibrational effects are noted for the structural parameters involving hydrogen: ∼20 mÅ for S−H, 4.3 mÅ for S−O, and 0.7° for ∠HSO. Once the electronic contribution is introduced, the geometry remains nearly unchanged, with the S−H bond length experiencing the largest effect: a decrease of about 0.2 mÅ to 1.3674(1) Å. The present SE equilibrium structure is accurate and offers the opportunity to derive accurate rotational constants for rare isotopologues, e.g. those containing ^{34}S, and thus support their observation both in the laboratory and in space. In this respect, it is important to stress the accuracy and reliability of r_e(SE)/r_e(SE)$_{full}$. In fact, the corresponding structural parameters have been found in very good agreement with those obtained, in ref. 125, at the CCSD(T)/CBS+CV+fT+fQ level (S−H = 1.3658 Å, S−O = 1.4937 Å, and ∠HSO = 104.59°).

The last radicals of Figure 3 are two isovalent species: HCO (right panel, top), which is the O-bearing analogous of HCS, and HSiO (right panel, bottom), which is obtained by replacing S with O and C with Si in HSC. For HCO, an important species in combustion chemistry and astrochemistry, only two isotopologues have been experimentally investigated: HCO and DCO. For all types of structures considered, the uncertainty on the angle is small: 0.03° for r_0 and 0.02/0.01° for r_e(SE)/r_e(SE)$_{full}$. However, while the r_e(SE) and r_e(SE)$_{full}$ values are very similar, 124.42° and 124.48°, respectively, the r_0 angle is about 0.5° larger (124.97°). A similar situation is observed for the CO bond, whose r_0 distance is 1.1797(1) Å and shortens by about 4 mÅ when moving to r_e(SE)/r_e(SE)$_{full}$, the corresponding values being 1.1762(1)/1.17612(6) Å. As expected (see discussion above), the C−H bond distance is the most affected by vibrational effects. The r_0 and r_e(SE) values are 1.1224(4) Å and 1.1178(3) Å, respectively, the former thus being ∼5 mÅ longer than the latter. Instead, electronic corrections do not affect significantly the bond length, the r_e(SE)$_{full}$ value being 1.1173(2) Å. To improve the r_e(SE) determination, the lack of important isotopic substitutions has to be overcome, thus calling for experimental measurements for the ^{13}C- and/or ^{18}O-substituted isotopic species. As mentioned for HSO, the availability of accurate SE equilibrium structures allows for getting accurate equilibrium rotational constants for missing isotopologues that, once corrected for vibrational effects, offer accurate predictions to be exploited for experiment guidance.

The last radical species of Figure 3 is SiOH. Its SE equilibrium structure has only been partially determined because, even though data for four isotopologues are available, these are limited to effective rotational constants ($B_{\rm eff}$), which were obtained by fitting SiOH transition frequencies to the linear molecule Hamiltonian, and thus $B_{\rm eff}$ can be considered the half sum of B_0 and C_0. This obviously led to the impossibility of deriving the ∠HSiO angle, which has been kept fixed at the best value available in the literature, i.e. 118.39° (from RCCSD(T)/cc-pV5Z calculations[170]). The r_0 structural parameters are: O−H = 0.970(1) Å and Si−O = 1.6475(1) Å. These values are in agreement with the determination carried out

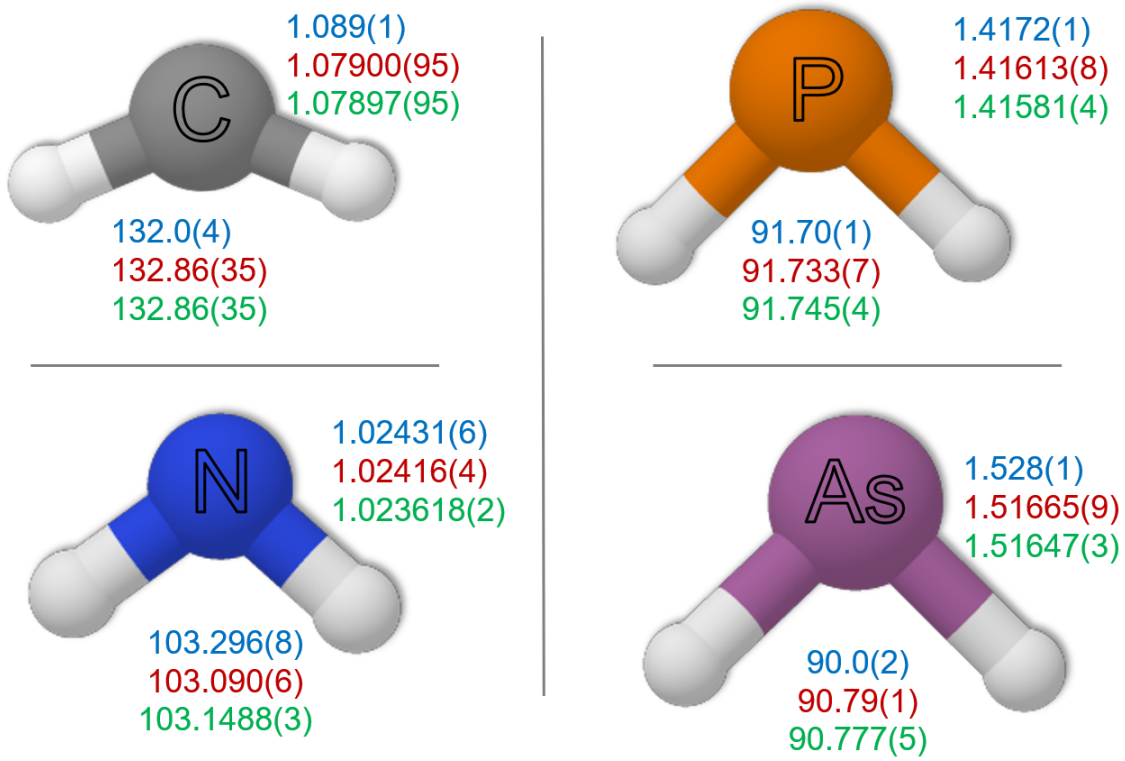

Figure 4: Triatomic radicals of C_{2v} symmetry considered in this work: r_0 (light blue), r_e(SE) (red), and $r_e(\mathrm{SE})_{full}$ (green) structures. Bond lengths are in Å, angles in degrees.

in ref. 111 (O−H = 0.969(4) Å and Si−O = 1.648(2) Å). To account for vibrational effects, the experimental ground-state B_{eff} constants ($(B_0 + C_0)/2$) have been corrected for the mean value of the corresponding vibrational corrections ($(\Delta B_{\mathrm{vib}} + \Delta C_{\mathrm{vib}})/2$). The resulting r_e(SE) C−H and Si−O bond lengths are 0.971(2) Å and 1.6440(1) Å, respectively. Both bond distances remain nearly unchanged when the electronic correction is incorporated, the changes being of the order of 1 mÅ. The last comment concerns the statistical errors, which are nearly the same for all types of structures.

Figures 4. In Figure 4, four radicals of C_{2v} symmetry and XH_2 general formula are collected. While the species with X = N, P and As are members of a family, X belonging to the same group of the periodic table, CH_2 has been considered as a separated molecule. For this latter, which is a radical of astrochemical interest, only two isotopologues have been

investigated using rotational spectroscopy: the parent species and the mono-deuterated variant (CDH). From the comparison reported in Figure 4, it is noted that vibrational effects are very pronounced. The r_0 C−H bond and ∠HCH angle are 1.089(1) Å and 132.0(4)°, respectively. When moving to r_e(SE), the CH bond length decreases to 1.07900(95) Å, i.e. by about 10 mÅ, while it remains nearly unchanged when incorporating the electronic contribution. A similar trend is observed for the angle, whose r_e(SE) and $r_e(\mathrm{SE})_{full}$ value is 132.86(35)°, the electronic corrections thus resulting entirely negligible. For comparison purposes, we note that the best computational study on CH_2, which –starting from CCSD(T) calculations with a large augmented-core-valence basis set (aug-cc-pCV6Z)– incorporated scalar relativistic effects, diagonal BO corrections and high-order electronic correlations (up to pentuples),[171] led to C−H = 1.075660 Å and ∠HCH = 133.922°. The largest difference with our results is observed for the C−H bond (about 3.3 mÅ). This comparison points out that even if only two isotopic species are available, an accurate and reliable r_e(SE) could be determined.

The NH_2, PH_2 and AsH_2 dihydrides provide insights into the structural modifications occurring when moving down along a group of the periodic table. In the case of NH_2, the experimental data include the rotational constants for NH_2, NHD and ND_2 for both ^{14}N and ^{15}N (see Table 1). In view of the large set of isotopologues and its planarity, NH_2 is a suitable test case for comparing the different possible choices of rotational constants to be employed in the LSQ fit. The results are summarized in Table 4. From its inspection, it is noted that, if only vibrational corrections are incorporated (r_e(SE)), the best possible combination of rotational constants (i.e. smaller uncertainties) is B_0/C_0, this being related to the α_2^A vibration-rotation interaction constants as previously discussed. For r_e(SE), the largest differences noted are between the results from the A_0/B_0 and B_0/C_0 sets for the bond distance, 0.35 mÅ, and between those from the A_0/B_0 and A_0/C_0 sets for the angle, 0.08°. Therefore, the differences are larger than the statistical errors, but are well within the typical estimated accuracy of SE equilibrium geometries (i.e. 1 mÅ for bond lengths and 0.1°

Table 4: SE equilibrium structures of the amidogen radical from different combinations of the rotational constants.

	r_e(SE)		$r_e(\mathrm{SE})_{full}$	
	N−H (Å)	∠HNH (°)	N−H (Å)	∠HNH (°)
A_0/B_0	1.024163(43)	103.0899(58)	1.023618(2)	103.1488(3)
B_0/C_0	1.023809(15)	103.1443(40)	1.023931(21)	103.1001(58)
A_0/C_0	1.023878(28)	103.0623(82)	1.023873(14)	103.1718(42)
$A_0/B_0/C_0$	1.023949(42)	103.0991(93)	1.023808(35)	103.1400(77)

for angles). Introduction of electronic corrections ($r_e(\mathrm{SE})_{full}$) varies in a nearly negligible manner the geometrical parameters (the largest changes are 1 mÅ on N−H for the A_0/B_0 and $A_0/B_0/C_0$ combinations, and 0.1° on ∠HNH for the A_0/C_0 set) and, on average, reduces the statistical uncertainties. While for the B_0/C_0 set, a small increase is observed, for the A_0/C_0 and $A_0/B_0/C_0$ combinations a small reduction is instead noted. Interestingly, for the A_0/B_0 set, the statistical errors decrease by one order of magnitude. More in detail, on the basis of the uncertainties on the structural parameters (from the largest to the smaller), the combinations order is the following: $A_0/B_0/C_0 > A_0/C_0 > B_0/C_0 > A_0/B_0$. Such an order reflects the accuracy of the experimental rotational constants used; indeed, as mentioned in the Methodology section, the accuracy order (from the most to the least accurate) is $A_0 > B_0 > C_0$. The last note concerns the $A_0/B_0/C_0$ combination, which is a redundant (linearly dependent) set of data: while the structural parameters obtained when using all the three rotational constants are accurate and reliable, their statistical uncertainties are larger than those resulting from LSQ fits that use only linearly independent data. This latter is an outcome of general validity. In the following, only the results from the LSQ fit using the A_0/B_0 set are considered (also reported in Figure 4).

For NH_2, some previous equilibrium geometries are available in the literature. The pure experimental and SE equilibrium structures have previously been determined using only the NH_2 parent species, the corresponding N−H distance being 1.0254(12) Å[172] and 1.0239(9) Å,[156] respectively. Our determination, based on the set of the six different isotopo-

logues mentioned above, led to a r_0 value of 1.02431(6) Å and $r_e(\mathrm{SE})/r_e(\mathrm{SE})_{full}$ values of 1.02416(4)/1.023618(2) Å. Because of the large uncertainties affecting the N−H bond lengths in refs. 156,172 (about 1 mÅ), they agree with our r_0 and r_e(SE) values. Instead, incorporation of the electronic corrections leads to a shortening of about 0.5 mÅ. Moving to the ∠HNH angle, the literature values based on the NH_2 isotopic species are 102.85(14)° (pure experimental determination[172]) and 103.10(6)° (SE equilibrium value[156]). For this angle, our 6-isopologue determination is 103.296(8)° for r_0, 103.090(6)° for r_e(SE) and 103.1488(3)° for $r_e(\mathrm{SE})_{full}$. All these values agree within 0.2°. Moving from r_0 to r_e(SE), the angle shrinks by about 0.2°, and then it widens by about 0.06° when accounting for electronic corrections. For both structural parameters, the uncertainties affecting our values are 1-2 orders of magnitude smaller than those of the literature results.[156,172] Finaly, we note that the CCSD(T)/CBS+CV+fT+fQ structure from ref. 62, with a N−H distance of 1.0237 Å and an angle of 103.18°, shows an agreement well within 1 mÅ and 0.1° with our SE equilibrium geometries. In conclusion, NH_2 provides another example of the great accuracy obtainable by applying the SE approach to radical species. Furthermore, incorporation of electronic corrections turns out a powerful tool to recover non-adiabatic effects due to a low-lying excited state.

For phosphidogen, the LSQ fit employed the data available for the three species containing only stable isotopes: PH_2, PHD, and PD_2. The resulting r_e(SE) is 1.41613(8) Å for P−H and 91.733(7)° for ∠HPH. Therefore, we note that the angle narrows when going from NH_2 to PH_2, with this being mainly related to the increased size of the central atom and its lone-pair when moving from N to P. An analogous –albeit less marked– trend is observed when going from PH_2 to AsH_2, the r_e(SE) angle of the latter being 90.79(1)°. Thus, it is expected that only negligible variations occur when moving further down along the periodic-table group. From the comparison of the $r_e(\mathrm{SE})_{full}$ structures, it is apparent that incorporation of electronic corrections is less and less important when going down along the group, indeed becoming negligible for the two heavier hydrides. For PH_2 and AsH_2,

the r_0 P−H and As−H bond lengths are 1.4172(1) Å and 1.528(1) Å, respectively, which shorten to 1.41581(4) Å and 1.51647(3) Å, respectively, in the case of $r_e(\mathrm{SE})_{full}$ (i.e. when vibrational and electronic contributions are considered in the LSQ fit). The corresponding angles are 91.745(4)° for PH_2 and 90.77(75)° for AsH_2. It is worthwhile noting that this is the first accurate equilibrium structure for AsH_2 reported in the literature so far. For PH_2, the CCSD(T)/CBS+CV+fT+fQ results from ref. 62, P−H = 1.4158 Å and ∠HPH = 91.78 °, are in nearly perfect agreement with our $r_e(\mathrm{SE})_{full}$ values.

Tetratomic species

The tetratomic radicals investigated in this work are shown in Figure 5, where the corresponding r_0, r_e(SE) and $r_e(\mathrm{SE})_{full}$ structures are also reported. All the radical species here considered are planar.

In the left panel of Figure 5, we find the trans (top) and cis (bottom) forms of HOCO. This radical is important in combustion processes and in the terrestrial atmosphere, where it plays a key role in converting CO into CO_2.[173] The trans form is more stable than the cis one by about 6 kJ/mol. Despite this energy difference, the same isotopologues could be experimentally investigated for both trans and cis forms.[140] These are, in addition to the parent species, DOCO, $H^{18}OCO$, $HOC^{18}O$, and $HO^{13}CO$.[140] A SE equilibrium structure for this species was reported for the first time in ref. 140, together with the r_0 geometry. The recommended values for the r_e(SE) structural parameters from ref. 140 are also reported (using pink color) in Figure 5 and compared with the results obtained in the present work. For both isomers, our r_e(SE) structures agree within the quoted errors with those reported in ref. 140. It has to be noted that the recommended values from ref. 140 have uncertainties that are one order of magnitude larger than ours only because conservative errors of 1 mÅ for bond lengths and 0.1° were applied to the former. The novelty of this work is the incorporation of the electronic corrections, which however have a negligible impact on the r_e(SE) parameters.

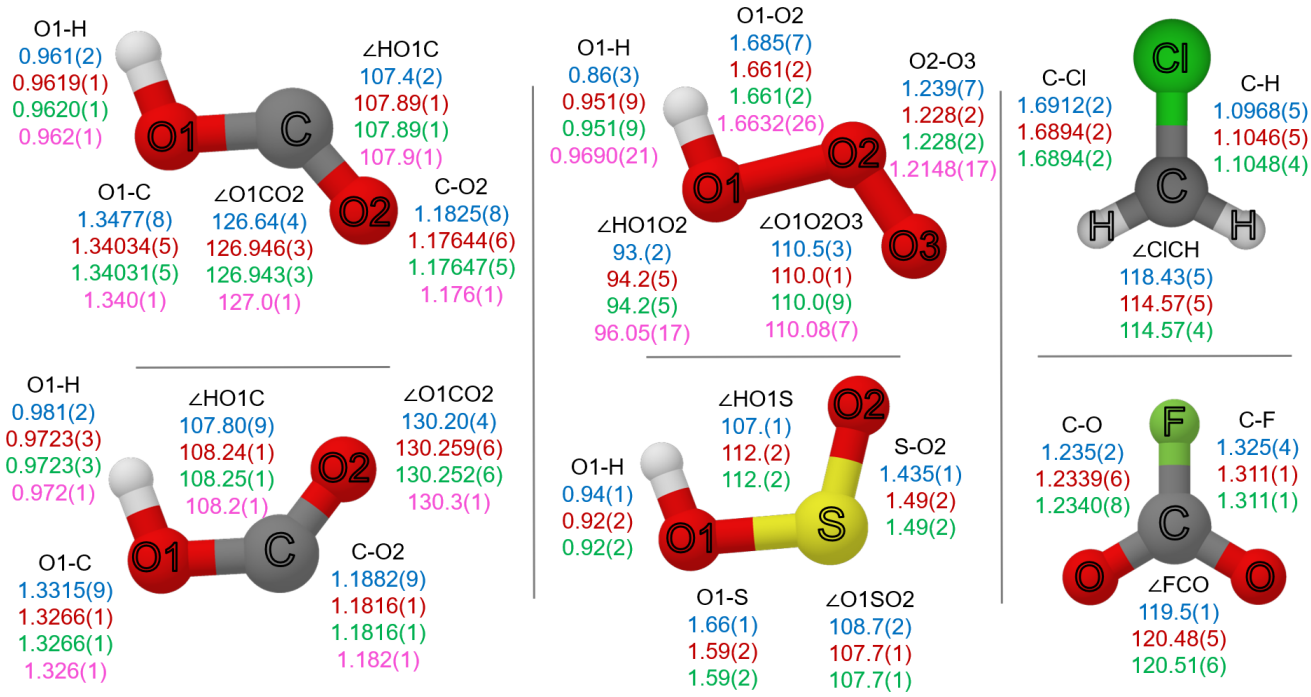

Figure 5: Tetratomic radicals considered in this work: r_0 (light blue), r_e(SE) (red), and $r_e(\mathrm{SE})_{full}$ (green) structures for the. The pink color refers to the recommended values from ref. 140 for the HOCO forms and from ref. 174 for HO_3. Bond lengths are in Å, and angles in degrees.

In the middle panel of Figure 5, two isovalent radicals are shown: HOOO (top) and HOSO (bottom). The HOOO radical is a challenging species: it can be considered as a molecule formed via weak interaction between the OH radical and the O_2 molecule. Several studies addressed the molecular structure of this species, with the most recent results being reported in 2019.[174] In ref. 174, the vibration-rotation interaction constants required to derive the vibrational corrections to rotational constants were obtained using a composite scheme denoted as focal point analysis (FPA).[175,176] The resulting r_e(SE) is: $O_1-H = 0.9690(21)$ Å, $O_1-O_2 = 1.6632(26)$ Å, $O_2-O_3 = 1.2148(17)$ Å, $\angle HO_1O_2 = 96.05(17)°$ and $\angle O_1O_2O_3 = 110.08(7)°$.[174] This r_e(SE) is their recommended equilibrium geometry and was evaluated using all the three rotational constants despite the planarity constraint (see eq. 7). These can be compared with our r_e(SE) (Figure 5: red color), which was instead obtained employing B_0 and C_0 in the LSQ fit. Focusing on the O_1-H bond length, our determination is 0.951(9) Å, thus about 18 mÅ shorter than the value above. However, if the SE equilibrium structure

obtained in ref. 174 using the B_0 and C_0 constants is considered, a good agreement is noted: 0.9521(36) Å vs 0.951(9) Å. Another r_e(SE) available in the literature (ref. 177) was determined using a multireference method (MRCI+Q), in conjunction with the aug-cc-pVTZ basis set, for computing vibrational corrections. For the O_1-H distance, they obtained a value of 0.961 Å, which agrees with both results within statistical uncertainties. A further SE equilibrium structure determination was reported in ref. 36, where the CCSD(T)/aug-cc-pVQZ level of theory was used for the evaluation of vibrational corrections. In that work, the LSQ fits employing different combinations of rotational constants were provided; the resulting O_1-H bond lengths range from 0.944 Å to 0.952 Å. Therefore, these results are in reasonable agreement with our determination, while they significantly deviate from the recommended value of ref. 174. Since the last two works discussed above (namely refs. 36,177) considered a set of isotopologues smaller than the one employed in ref. 174 and in our study, the most meaningful comparison is that with the results from ref. 174. The last comment on the O_1-H bond concerns r_0. As already noted in previous works,[36,139] a very short bond distance is obtained when the r_0 structure is considered (0.86 Å), which was attributed to the HO_3 torsional mode. Moving to the other bond lengths, namely O_1-O_2 (central O–O bond) and O_2-O_3 (terminal O–O bond), sensible deviations from the literature are noted. For O_1-O_2, our SE value of 1.661(2) Å is in good agreement with that from ref. 174 (1.6632(36) Å), the difference of 2 mÅ being well within the statistical uncertainties. For O_2-O_3, the difference is more pronounced: our determination is 1.228(2) Å and thus is 13 mÅ longer than the recommended value (1.2148(17) Å) from ref. 174. We tried different combinations of rotational constants in the LSQ fit, but we were unable to reproduce that result: in all cases, a bond length longer by at least 10 mÅ was obtained. The comparison for angles points out that we predict a $\angle HO_1O_2$ angle smaller by about 2° than that from ref. 174: 94.2(5) vs 96.02(17)°. Instead, for the $\angle O_1O_2O_3$ angle the difference is only 0.1°, 110.0(9)° vs 110.08(7)°, thus well within the given uncertainties. The deviations from the literature values cannot be ascribed to the different methodologies employed for

the computation of the vibrational corrections;[25] instead, as already noted in ref. 36, the combination of rotational constants employed in the LSQ fit affects the final outcome. If we compare our results (B_0/C_0 combination) with those from ref. 174 that made use of same set of rotational constants (i.e. r_e(BC) in Table VI[174]), the agreement for O_1-O_2 still persists. Finally, incorporation of the electronic corrections in the LSQ fit does not provide any noticeable improvement.

The cis (also denoted as *syn*) form of the HOSO radical is another challenging radical, which plays a role in combustion, atmospheric and interstellar chemistry.[37] According to the fc-CCSD(T)/cc-pVTZ computations we carried out, this species is planar, and thus its planarity has been assumed in this work. However, in the literature its non-planarity has been discussed at length.[37] All the structures addressed in the following have been obtained by fitting the B_0 and C_0 rotational constants. If no vibrational corrections are considered in the LSQ fit, the r_0 structure (see Figure 5) is obtained, which can be compared with that of ref. 37. From such a comparison it is noted that the two structures essentially agree within the provided uncertainties. Indeed, our r_0 $H-O_1$ and O_1-S distances are 0.94(1) Å and 1.66(1) Å, respectively, which well match the values of 0.932(15) Å and 1.657(9) Å from ref. 37. Instead, a difference is noted for the $S-O_2$ bond: our value of 1.435(1) Å is 8 mÅ shorter than that of ref. 37 (1.443(9) Å), which is however affected by a larger uncertainty. Moving to r_e(SE), we first of all note that the LSQ fit resulted problematic, with large residuals which do not improve by introducing the electronic corrections. The general conclusion is that it is not possible to define an equilibrium structure able to accurately reproduce the rotational constants of all the different isotopic species. The overall conclusion is that the molecule is planar on the vibrational ground state, but it is not at the bottom of the potential energy well. A small deviation of the system from planarity is expected to also affect the accuracy of the computed vibrational corrections. However, our LSQ fit suggests that the experimental results should be reviewed for the doubly ^{18}O-substituted isotopic species. In fact, we could only incorporate the B_0 constant in the fit, while A_0 and B_0 could not at all be reproduced.

Finally, a detailed comparison between the r_0 and $r_e(\mathrm{SE})/r_e(\mathrm{SE})_{full}$ structural parameters is meaningless because of the large uncertainties of about 10-20 mÅ for bond lengths and 0.1°-0.2° for angles affecting the SE geometries.

The last two radicals appearing in Figure 5 (right panel) are FCO_2 (top) and $ClCH_2$ (bottom), which are both planar with C_{2v} symmetry. The best structure reported in the literature for FCO_2 was obtained in ref. 136, where both r_0 and r_s structures were determined. The former can be compared with the present determination: our r_0 C−F and C−O bond lengths are 1.325(4) Å and 1.235(2) Å, respectively, which agree rather well with the values of 1.3204 Å and 1.2407 Å from ref. 136, the differences being about 5 mÅ for both bond lengths. Moving to the SE equilibrium structure, it is noted that the differences between r_e(SE) and $r_e(\mathrm{SE})_{full}$ are entirely negligible. Indeed, the effect of electronic corrections is smaller than 0.01 mÅ for bonds and about 0.03° for the ∠FCO angle. The $r_e(\mathrm{SE})_{full}$ structural parameters are: C−F = 1.311(1) Å, C−O = 1.2340(8) Å, and ∠FCO = 120.51(6)°. The comparison of these values with the r_0 ones points out a shortening of 14 mÅ for C−F when moving to equilibrium, while the difference for C−O is only 1 mÅ. A noticeable enlargement of 1° is observed for ∠FCO when going from r_0 to r_e. Finally, our results agree within 1-5 mÅ with the corresponding r_s values;[136] however, as discussed in the Introduction, the r_e(SE) structure is more reliable than its r_s counterpart. Therefore, our study provides the most accurate structure of FCO_2 available so far; furthermore, its accuracy is such that it can be employed to derive the rotational constants for the ^{13}C-containing isotopologue, which has not experimentally been characterized yet.

All the structures of $ClCH_2$ reported in Figure 5 have been obtained from the data available for only two isotopic species: $^{35}ClCH_2$ and $^{37}ClCH_2$.[138] In ref. 138, in addition to the characterization of the rotational spectra of these two isotopologues, the r_0 structure was provided. The authors assumed a C−H bond distance of 1.09(1) Å and, by fitting the vibrational ground-state rotational constants, they derived C−Cl = 1.691(4) Å and ∠HCH = 122.6(2)° (this implying ∠ClCH = 118.7°).[138] In our r_0 determination, we let instead

the C−H bond length vary and determined all the three parameters. Despite the lack of any isotopic substitution at the hydrogens, the fit led to a r_0 geometry in agreement with the literature one, but improved in terms of uncertainties: C−H = 1.0968(5) Å, C−Cl = 1.6912(2) Å and ∠ClCH = 118.43(5)° (this implying ∠HCH = 123.14°). Moving to r_e(SE), the missing information on the isotopic substitution for the H atoms leads to a suspicious longer distance for C−H, 1.1046(5) Å, and the ∠ClCH seems to decrease too much. Indeed, these structural parameters are strongly correlated in the LSQ fit. Therefore, without further experimental data we cannot estimate the reliability of the r_e(SE) parameters and improve them. Incorporation of electronic corrections has negligible effects on both the structural parameters and their uncertainties.

The "Lego-brick" approach at work

As mentioned in the Introduction, the "Lego-brick" approach can be employed to obtain accurate equilibrium structures at a low computational cost. It can also be used to provide reliable estimates for structural parameters that need to be kept fixed in partial SE determination. To the best of our knowledge, this is the first application of the "Lego-brick" approach to radical species. As mentioned in the Methodology section, two different procedures have been tested: "parent_molecule–radical TM" and "radical–radical TM".

The "parent_molecule–radical TM" approach

In Figure 1, the systems considered for the "parent_molecule–radical TM" approach are depicted: benzene has been employed to template the phenyl radical, vinyl cyanide (acrylonitrile) for the trans and cis forms of the β-cyanovinyl radical, vinyl chloride for the trans-β-chlorovinyl radical, acrolein for s-trans-CH_2CHCO, and propadienone for linear-CH_2CHCO. This test was kept limited because we expected that the strong electronic modifications occurring when a closed-shell molecule homolytically looses a hydrogen atom, are not reliably accounted for in the TM approach. Furthermore, several systematic studies have shown that,

Table 5: Comparison of experimental and computed ground-state rotational constants (MHz) at the revDSD/junTZ level and from the "parent_molecule–radical TM" (TM) approach.

trans-β-cyanovinyl radical						
	Experiment[a]	revDSD	Error (%)	TM	Error(%)	$\Delta B_{\rm vib}$[b]
A_0	65918.10(53)	66621.02	1.07	66327.43	0.62	-257.56
B_0	5067.06(59)	5067.73	0.01	5098.11	0.61	2.54
C_0	4685.71(57)	4701.44	0.34	4726.15	0.86	8.95
cis-β-cyanovinyl radical						
	Experiment[a]	revDSD	Error (%)	TM	Error(%)	$\Delta B_{\rm vib}$[b]
A_0	49757.42(27)	49622.57	-0.27	49479.09	-0.56	-221.47
B_0	5364.31(16)	5395.68	0.58	5430.82	1.24	6.245
C_0	4832.54(13)	4856.87	0.50	4884.00	1.07	12.58
phenyl radical						
	Experiment[c]	revDSD	Error (%)	TM	Error(%)	$\Delta B_{\rm vib}$[b]
A_0	6280.203(113)	6397.29	1.86	6419.74	2.22	42.78
B_0	5599.597(92)	5707.55	1.93	5728.54	2.30	41.37
C_0	2959.40114(57)	3017.36	1.96	3028.21	2.33	22.04
trans-β-chlorovinyl radical						
	Experiment[d]	revDSD	Error (%)	TM	Error(%)	$\Delta B_{\rm vib}$[b]
A_0	57457.5039(13)	58656.45	2.09	58642.79	2.06	-328.16
B_0	6483.86279(30)	6427.06	0.88	6493.83	0.15	47.03
C_0	5816.07623(31)	5782.39	0.58	5836.29	0.35	44.91
s-trans-CH_2CHCO						
	Experiment[e]	revDSD	Error (%)	TM	Error(%)	$\Delta B_{\rm vib}$[b]
A_0	60392.2023(21)	60565.82	0.29	60590.49	0.33	543.20
B_0	4654.42551(55)	4635.65	0.40	4663.52	0.20	21.01
C_0	4322.76810(36)	4306.64	0.37	4330.82	0.19	20.29
linear-CH_2CHCO						
	Experiment[e]	revDSD	Error (%)	TM	Error(%)	$\Delta B_{\rm vib}$[b]
A_0	48845.53592(146)	48836.30	0.02	49177.01	0.68	459.47
B_0	4753.70918(38)	4737.85	0.33	4751.55	0.05	3.06
C_0	4327.29901(45)	4324.97	0.31	4327.99	0.02	11.00

[a] Taken from ref. 68. [b] Computed at the revDSD/junTZ level of theory. [c] Taken from ref. 67. [d] Taken from ref. 178: ^{35}Cl-isotopologue. [e] Taken from ref. 179.

for closed-shell species, the equilibrium bond lengths computed using the revDSD functional are systematically too long, with this providing a general explanation why the LR, TM, and related approaches are so successful.[180,181] The situation is however different for open-shell systems: for them, the revDSD functional tends to underestimate the equilibrium bond lengths. To give an example, the revDSD/junTZ C−C equilibrium bond length in benzene (1.3941 Å) is overestimated by about 3 mÅ with respect to its r_e(SE) value (1.3916(1) Å[25]), whereas the revDSD/junTZ C−C bond distances in the phenyl radical (C_i−C_o = 1.3678 Å, C_o−C_m = 1.3953 Å, C_m−C_p = 1.3881 Å) are underestimated, on average, by 5 mÅ with respect to their r_e(SE) counterparts (C_i−C_o = 1.3731(47) Å, C_o−C_m = 1.3980(17) Å, C_m−C_p = 1.3927(16) Å[25]). Therefore, the general rule seems to be that the systematic corrections go in opposite directions for closed-shell and open-shell species, thus preventing the application of the TM approach.

Our expectation is confirmed by the results collected in Table 5, where the experimental and computed ground-state rotational constants are compared. In the last column of Table 5, the vibrational corrections required to correct the equilibrium rotational constants, straightforwardly derived from the TM geometry, are reported. It has to be noted that, in the present case, the "Lego brick" is the entire molecule; thus, there is no LR correction to apply and the "Lego-brick" approach is the TM approach itself. From the inspection of Table 5, it is apparent that deviations from experiment increase when moving from the revDSD/junTZ level to the TM-approach results: on average, for the β-cyanovinyl radical: from 0.46% to 0.83%, for the phenyl radical: from 1.92% to 2.28%, and for the CH_2CHCO radicals: from 0.29% to 0.37%. Only for the trans-β-chlorovinyl radical we note a slight improvement: on average from 1.18% to 0.85%. However, these deviations are much larger than what expected from the TM approach. In Table S2 of the SI, the corresponding results obtained by applying the TM approach to B2PLYP/junTZ calculations are collected. It is noted that the outcome is very similar to that of Table 5 both at the DFT and TM level. We can therefore conclude that, as expected, the disappointing results of Table 5 are

Table 6: TM bond lengths (in Å)[a] and corresponding rotational constants (in MHz) for the C_nS species with n = 4, 6, 8, and 10.

Parameter	C_4S	C_6S	C_8S	$C_{10}S$
r(C1S)	1.5576	1.5571	1.5573	1.5584
r(C1C2)	1.2798	1.2804	1.2805	1.2801
r(C2C3)	1.2908	1.2806	1.2786	1.2779
r(C3C4)	1.2937	1.2726	1.2753	1.2764
r(C4C5)		1.2938	1.2824	1.2796
r(C5C6)		1.2862	1.2691	1.2723
r(C6C7)			1.2960	1.2841
r(C7C8)			1.2817	1.2661
r(C8C9)				1.2973
r(C9C10)				1.2789
B_e(TM)	1518.42	596.73	297.42	170.29
B_0(TM) [b]	1518.77 (0.03%)	597.18 (0.01%)	297.93 (0.04%)	170.83
B_0(exp) [c]	1519.2062(3)	597.12499(7)	297.81(1)	-

[a] Angles are kept fix at 180°. [b] Computed vibrational corrections to rotational constants are: at the fc-CCSD(T)/cc-pVTZ level for the C_4S species, and at the fc-MP2/cc-pVDZ level for longer chain (C_6S, C_8S, and $C_{10}S$). [c] Experimental values taken from ref. 71.

not related to the choice of the double-hybrid functional employed for the initial structural determination.

The "radical–radical TM" approach

The systems considered in the "radical–radical TM" approach are shown in Figure 2. In this model, a radical species is used for describing the radical center of a larger open-shell species. The first example considered is the C_nS system[†], with n = 4, 6, 8 and 10. As shown in Figure 2, the "bricks" considered are the C_2S radical, and the C_3S and C_5S closed-shell molecules. Following the color code employed in Figure 2 (and in particular the colored halos), C_4S can be seen as resulting from the combination of the C_2S radical and the terminal CC fragment of C_3S (C2C3, the numbering of the C atoms starting from the closest one to S). Moving

[†]For n = odd, C_nS is a closed-shell molecule; for n = even, C_nS is a open-shell species with a $^3\Sigma^-$ electronic ground state.

to C_6S, the three envisaged fragments are the C_2S radical, the central CC moiety of C_5S (C2C3, where the numbering of the C atoms again starts from the closest one to S), and the terminal CC fragment of C_3S. C_8S and $C_{10}S$ are obtained by adding to the fragments used for C_6S, one and two additional central CC moieties of C_5S, respectively. As explained in the Methodology section, the TM approach has been employed for the fragments and the LR one to correct the linkage between the fragments. For the sake of brevity, TM is used to denote the application of the TM approach only, while TM+LR denotes the additional consideration

Table 7: TM[a] bond lengths (in Å) and corresponding rotational constants (in MHz) for the CH_2CHCO radicals.

Parameter	linear-CH_2CHCO	s-trans-CH_2CHCO
r(C1C2)	1.4143	1.3332
r(C1H3)	1.0762	1.0805
r(C1H4)	1.0748	1.0798
r(H5C2)	1.0813	1.0846
r(C6C2)	1.3322	1.4760
r(C6O8)	1.1620	1.1849
∠(H3C1C2)	121.09	120.32
∠(H4C1C2)	118.98	121.41
∠(H5C2C1)	121.39	122.55
∠(C6C2C1)	124.79	119.91
∠(O8C6C2)	179.70	128.28
A_e (TM)	49456.77	61026.45
B_e (TM)	4762.48	4675.37
C_e (TM)	4344.16	4342.67
A_0 (TM) [b]	48997.30 (0.31%)	60483.25 (0.15%)
B_0 (TM) [b]	4759.42 (0.12%)	4654.36 (0.001%)
C_0 (TM) [b]	4333.16 (0.14%)	4322.38 (0.01%)
A_0 (exp) [c]	48845.5359(15)	60392.2030(21)
B_0 (exp) [c]	4753.70918(38)	4654.42551(55)
C_0 (exp) [c]	4327.29901(45)	4322.76810(36)

[a] Ethene and the HCO radical employed for the TM approach. [b] Computed vibrational corrections to rotational constants are at the revDSD/junTZ level. [c] Experimental values taken from ref. 179.

of the LR approach. However, as in the case of the "parent_molecule–radical" strategy, the LR correction is expected to go in the wrong direction. While the r_e(SE) structure of C_2S is shown in Figure 3, those of C_3S and C_5S are reported in the SI (Table S4), with that of C_5S being purposely obtained in this work. In the SI, the revDSD/junTZ optimized geometries are also reported. The resulting TM equilibrium structures for the C_nS radicals, with n = 4, 6, 8 and 10, are given in Table 6 together with the corresponding equilibrium rotational constants, while the corresponding TM+LR results are provided in Table S5 of the SI. The TM and TM+LR B_e values have been augmented by vibrational corrections (at the CCSD(T)/cc-pVTZ level for C_4S and MP2/cc-pVDZ for the other radicals), thus obtaining the computational estimates of the ground-state rotational constants to be compared with experiment. For the pure TM approach, the agreement is impressive (see Table 6), with deviations that range from 0.01% to 0.04%, and are thus improved by one order of magnitude with respect to the estimates at the revDSD/junTZ level (see Table S3 in the SI). This outcome is in line with the benchmark of the "Lego-brick" approach carried out for small PA(N)Hs.[66] For $C_{10}S$, there are no experimental data available and, therefore, our TM B_0 is expected to provide a very accurate prediction with a conservative uncertainty of 0.05%. From an inspection of Table S5, we note that, moving from TM to TM+LR, the relative deviation with respect to experiment increases by one order of magnitude, the only exception being C_4S, whose TM+LR relative difference is only twice the corresponding TM one.

In Table 7, the outcomes the "radical–radical" TM strategy applied to the CH_2CHCO radicals are reported. As somewhat expected, the results are very good for s-trans-CH_2CHCO, but not so great for linear-CH_2CHCO. For the former, the mean relative deviation from the experimental ground-state rotational constants is 0.05%, while this increases to 0.19% for the latter radical. Indeed, from the inspection of Figure 2 and as noted in ref. 179, the radical center is on the CO moiety in the case of s-trans-CH_2CHCO, while it lies on the CH_2 frame for linear-CH_2CHCO. Therefore, the 'ethene + HCO' fragments are suitable for the former, but not for the latter. In the SI (Table S6), the results for the TM+LR approach

Table 8: Computed equilibrium and vibrational ground-state rotational constants (MHz) of the 1- and 2-naphthyl radicals.[a]

	1-naphthyl radical			2-naphthyl radical		
	revDSD[b]	TM (b)[c]	TM (b+a)[d]	revDSD[b]	TM (b)[c]	TM (b+a) [d]
A_e	3178.779	3168.568	3167.706	3320.117	3312.262	3310.853
B_e	1294.451	1293.590	1293.518	1246.460	1244.888	1245.508
C_e	919.866	918.589	918.467	906.235	904.819	905.041
A_0[e]	3156.052	3145.841	3144.979	3296.162	3288.307	3286.898
B_0[e]	1286.571	1285.710	1285.638	1238.948	1237.376	1237.996
C_0[e]	914.135	912.844	912.736	900.634	899.218	899.440

[a] 1 and 2 refer to the position of the radical center; see Figure 2. [b] revDSD stands for the revDSD/junTZ level of theory. [c] "b" in parentheses means that the TM approach has been applied only to bond lengths. [d] "b+a" in parentheses means that the TM approach has been applied to bond lengths and valence angles. [e] Vibrational corrections at the B3LYP-D3BJ/jun-cc-pVDZ level.

are provided. Based on the discussion above, it is not surprising that they are worse than the TM ones, with the worsening being more pronounced for s-trans-CH_2CHCO. Indeed, the averaged relative TM+LR difference from experiment is 0.30% for linear-CH_2CHCO (i.e. ∼1.5 times larger than that of TM) and 0.19% for s-trans-CH_2CHCO (i.e. ∼4 times larger than that of TM).

Based on the successful application of the "Lego-brick" approach to small PAHs[66] and on the promising results obtained for its "radical–radical TM" variant applied to the C_nS (n=4,6,8) system and s-trans-CH_2CHCO, the latter approach has been applied to the accurate prediction of the equilibrium structure and rotational constants for the 1- and 2-naphthyl radicals. As shown in Figure 2, the two fragments considered are benzene and the phenyl radical[‡]. For this system, there are no linkage bonds; therefore, the "Lego-brick" approach reduces to the TM model in the "radical–radical TM" variant. This latter has been applied to only the bond lengths (TM (b)) and to both bond distances and valence angles (TM (b+a)): while the equilibrium structures are reported in the SI, the corresponding equilibrium rotational constants are collected in Table 8 (second and third column for each radical,

[‡]For phenyl, the r_e(SE) structure obtained using the CCSD(T)/ANO0 vibrational corrections from ref. 67 (reported in ref. 33) was considered.

respectively). In this table, the revDSD/junTZ results are also provided for comparison purposes (first column). The ground-state rotational constants, obtained by adding the vibrational corrections computed at the B3LYP/jun-cc-pVDZ level, are also given in Table 8. For the 1-naphthyl radical, the "TM (b)" and "TM (b+a)" approaches provide very similar rotational constants: the differences are ∼0.85 MHz for A_0, ∼0.08 MHz for B_0 and ∼0.1 MHz for C_0. These differences, in relative terms, range from 0.01% to 0.03%, which are of the order of the expected uncertainties associated with the TM approach (in line with what obtained in ref. 66). For the 2-naphthyl radical, the differences are a bit larger, i.e. ∼1.4 MHz for A_0, ∼0.6 MHz for B_0 and ∼0.2 MHz for C_0, but still very small in relative terms: 0.02%-0.05%. Since in ref. 66 the TM approach was applied only to the distances, with the angles kept fixed at the DFT level, this tends to recommend the "TM (b)" results. While there are not experimental data to confirm such a recommendation, several systematic studies have shown that valence and dihedral angles optimized at the revDSD/junTZ level do not require any *a posteriori* correction.[78,180,181] In any case, it is surely encouraging that the 'TM (b)" and "TM (b+a)" approaches lead to very similar results. In the absence of any experimental information, with the aim of supporting laboratory work, we suggest to take their mean values and consider them affected by a conservative relative error of 0.05%.

Resonance-stabilized π-radicals

The "Lego-brick" approach is expected not to work for those radicals that show a delocalization of the unpaired electron(s). However, if the resonance structures can be reproduced and suitably weighted, the "radical–radical TM" approach might be successful. Still, the LR corrections cannot be taken into consideration based on the considerations of the previous sections. As mentioned at the beginning of the Methodology section, the propargyl radical has been chosen as test case to investigate the TM approach for resonance-stabilized radicals.

As shown in Figure 6, the propargyl radical has two resonance limits: the ethynyl methyl and allenyl structures. In ref. 32, the rotational spectrum of the propargyl radical has been

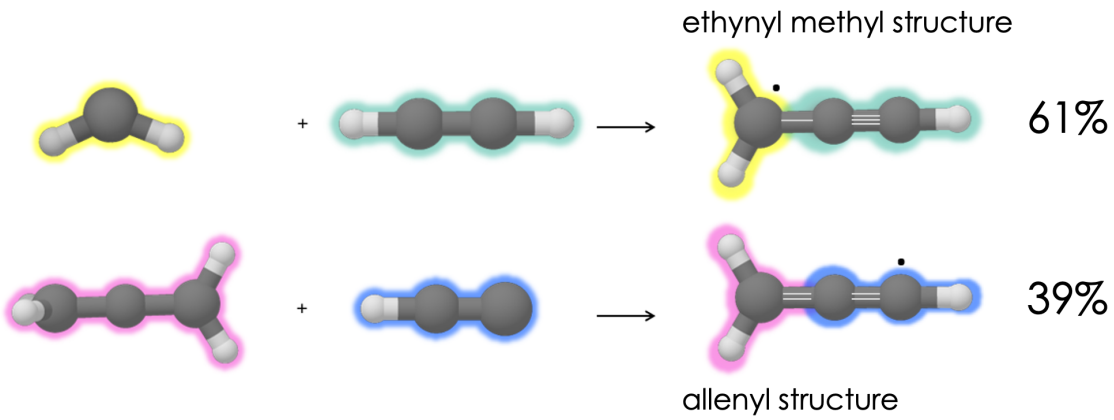

Figure 6: The "radical–radical TM" approach applied to the ethynyl methyl and allenyl resonance forms of the propargyl radical. Colored halos are use to highlight the TM fragments within the radical species.

investigated for nine isotopic species and its SE equilibrium structure accurately determined. Furthermore, in ref. 32, the experimental hyperfine coupling constants were employed to derive an accurate estimate of spin populations, these being used to evaluate the contributions of the two resonance structures reported in Figure 6. In this study, the "radical–radical TM" approach has been employed to provide an accurate description of the two resonance forms. For the ethynyl methyl radical, the CH_2 radical and acetylene[50] have been employed, the latter for the description of the CCH fragment. For the allenyl form, allene has been used for the CH_2 fragment[50] together with the CCH radical.[182] The TM equilibrium rotational constants of these two resonance structures are collected in Table 9 together with their weighted combination according to the percentages reported in Figure 6 (61% ethynyl methyl + 39% allenyl from ref. 32). These latter rotational constants, denoted as "weighted mean", are also compared with the SE equilibrium rotational constants from ref. 32. From the inspection of Table 9, it is noted that none of the two resonance forms is able to accurately describe the molecular structure of the propargyl radical, with an average deviation of 0.35% for rotational constants. Instead, weighting their contribution ("weighted mean") leads to rotational constants that are in very good agreement with the SE counterparts. In particular, for B_e

Table 9: TM equilibrium rotational constants (MHz) of the propargyl radical and their relative deviations (%) from the SE counterpart.

	TM propargyl radical			SE[a]
	ethyl methyl[b]	allenyl[c]	"weighted mean"[d]	
A_e (%dev.)	288467.1 (0.49%)	290073.8 (0.07%)	289093.7 (0.27%)	289878.1
			–	–
B_e (%dev.)	9556.0 (0.22%)	9481.9 (0.56%)	9527.1 (0.08%)	9534.9
			(0.08%)	9535.1
C_e (%dev.)	9249.6 (0.20%)	9181.7 (0.54%)	9223.1 (0.09%)	9231.2
			(0.09%)	9231.6

[a] From ref. 32. Upper line: rotational constants from the r_e(SE) structure. Lower line: SE equilibrium rotational constants obtained from the experimental values corrected for vibrational effects at the CCSD(T)/cc-pCVQZ level (all electron correlated). [b] The CH_2 radical and acethylene for the TM approach. [c] The CCH radical and allene for the TM approach. [d] 61% of the TM "ethyl methyl" and 39% of the TM "allenyl".

and C_e, which are those determined in the spectroscopic investigation, the match is well within 0.1%. Such an accuracy is usually obtained by exploiting composite schemes rooted in the coupled cluster theory.[168,183] Finally, it has to be noted that the contribution of each resonance form to the delocalized radical can be evaluated theoretically, thus not requiring a preliminary spectroscopic study. For example, in ref. 184, the contributions of the ethynyl methyl and allenyl structures were determined to be 65% and 35%, respectively, on the basis of atomic partitioning of the spin using Mulliken populations (spin density computed at the CCSD(T)/ANO level).

Concluding remarks

In summary, the very first systematic application to radicals of the semi-experimental approach for the determination of accurate equilibrium structures has been reported. A thorough analysis of the results together with a discussion also based on the comparison with literature data pointed out that this is a powerful approach even for open-shell species, with no degradation of accuracy with respect to the treatment of closed-shell species. Indeed, as

already noted for the latter, the statistical errors reduce when moving from r_0 to r_e(SE) and they are such that an accuracy better than 1 mÅ for bond lengths is obtained. While, in most cases, incorporation of electronic corrections only improves the statistical errors, in a few cases, when non-adiabatic effects are important, this leads to contributions of a few mÅ, which are non-negligible in view of the typical accuracy of SE equilibrium structures.

The main limitation faced in our systematic study is the number of data available. Indeed, open-shell species are not only challenging systems from a quantum-chemical point of view, but their instability and reactivity strongly hamper the experimental characterization. As a consequence, our benchmark work was limited to small radicals ranging from diatomics to tetratomic species. To overcome such a limitation and to provide results of similar accuracy to what obtainable with the semi-experimental approach, the applicability of this latter has been extended by exploiting the so-called "Lego-brick" approach. In this framework, we have devised the "radical–radical TM" variant, which seems to be very promising. Indeed, albeit limited in number, our results suggest that this model is able to obtained rotational constants with a relative accuracy well within 0.05%, which corresponds to uncertainties smaller than 1 mÅ for bond lengths.[1] The "radical–radical TM" seems to provide results in line with those obtained with the "Lego-brick" strategy applied to closed-shell species. However, it presents three major limitations. First of all, the suitable fragment should be available, as demonstrated from the CH_2CHCO radicals. Second, because of different trends in the systematic errors occurring in double-hybrid functional calculations for open- and closed-shell species, the LR approach worsens the results and only the TM model can be successfully exploited. Lastly, it is not able to well describe resonance-stabilized radicals, except for those cases that have well-defined resonance structures that can be reproduced and properly weighted.

Acknowledgement

This work has been supported by MUR (PRIN Grant Numbers 202082CE3T and P2022ZFNBL) and by the University of Bologna (RFO funds). The COST Action CA21101 "COSY - Confined molecular systems: from a new generation of materials to the stars" is acknowledged. The Skies-Village reference center of INSTM is acknowledged for providing high-performance computing facilities.

Supporting Information Available

In the SI the following information are reported: 1) Standard deviations of the LSQ fits. 2) The rotational constants obtained at the B2PLYP/junTZ level for the molecules of the "parent_molecule-radical" approach together with the rotational constants resulting from the application of the TM approach. 3) The revDSD/junTZ geometries for the C_nS family of radicals, with n = 2-6, 8 and 10. 4) The r_e(SE) structure of C_5S and C_3S. 5) The results for the TM+LR approach applied to C_nS and CH_2CHCO. 6) The revDSD/junTZ, "TM (b)" and "TM (b+a)" equilibrium geometries of the 1- and 2-naphthyl radicals.

References

(1) Puzzarini, C.; Stanton, J. F. Connections between the Accuracy of Rotational Constants and Equilibrium Molecular Structures. *Phys. Chem. Chem. Phys.* **2023**, *25*, 1421–1429.

(2) Gordy, W.; Cook, R. L. In *Microwave Molecular Spectra, 3rd Edition*; Weissberger, A., Ed.; Wiley: New York, 1984.

(3) Pulay, P.; Meyer, W.; Boggs, J. E. Cubic Force Constants and Equilibrium Geometry of Methane from Hartree–Fock and Correlated Wavefunctions. *J. Chem. Phys.* **1978**, *68*, 5077–5085.

(4) Demaison, J. Experimental, Semi-Experimental and Ab Initio Equilibrium Structures. *Mol. Phys.* **2007**, *105*, 3109–3138.

(5) Puzzarini, C.; Stanton, J. F.; Gauss, J. Quantum-Chemical Calculation of Spectroscopic Parameters for Rotational Spectroscopy. *Int. Rev. Phys. Chem.* **2010**, *29*, 273–367.

(6) Demaison, J., Boggs, J. E., Császár, A. G., Eds. *Equilibrium Molecular Structures: From Spectroscopy to Quantum Chemistry*; CRC Press, Taylor & Francis Group: Boca Raton, FL, US, 2011.

(7) Mills, I. M. Molecular Spectroscopy: Modern Research, ed. KN Rao and CW Matthews. 1972.

(8) Born, M.; Oppenheimer, R. Zur Quantentheorie der Molekeln. *Ann. Phys. (Berl.)* **1927**, *389*, 457–484.

(9) Woods, R. C.; Saykally, R. J.; Anderson, T. G.; Dixon, T. A.; Szanto, P. G. The Molecular Structure of HCO^+ by the Microwave Substitution Method. *J. Chem. Phys.* **1981**, *75*, 4256–4260.

(10) Puzzarini, C.; Tarroni, R.; Palmieri, P.; Carter, S.; Dore, L. Accurate Ab Initio Prediction of the Equilibrium Geometry of HCO^+ and of Rovibration Energy Levels of DCO^+. *Mol. Phys.* **1996**, *87*, 879–898.

(11) Costain, C. C. Determination of Molecular Structures from Ground State Rotational Constants. *J. Chem. Phys.* **1958**, *29*, 864–874.

(12) Kraitchman, J. Determination of Molecular Structure from Microwave Spectroscopic Data. *Am. J. Phys.* **1953**, *21*, 17–24.

(13) Demaison, J.; Rudolph, H. When Is the Substitution Structure Not Reliable? *J. Mol. Spectrosc.* **2002**, *215*, 78–84.

(14) Botschwina, P.; Puzzarini, C. CCSD(T) Spectroscopic Constants and an Accurate Equilibrium Structure for HC_4F. *J. Mol. Spectrosc.* **2001**, *208*, 292–294.

(15) Watson, J. K.; Roytburg, A.; Ulrich, W. Least-Squares Mass-Dependence Molecular Structures. *J. Mol. Spectrosc.* **1999**, *196*, 102–119.

(16) Cazzoli, G.; Cludi, L.; Contento, M.; Puzzarini, C. Rotational Spectrum of $CH_3C^{13}CCCH$: Determination of the Equilibrium Structure of Methyldiacetylene from Microwave Spectroscopy and Ab Initio Calculations. *J. Mol. Spectrosc.* **2008**, *251*, 229–234.

(17) Guarnieri, A.; Demaison, J.; Rudolph, H. D. Structure of Ketene – Revisited r_e (Equilibrium) and r_m (Mass-Dependent) Structures. *J. Mol. Struct.* **2010**, *969*, 1–8.

(18) Demaison, J.; Császár, A. G.; Margulès, L. D.; Rudolph, H. D. Equilibrium Structures of Heterocyclic Molecules with Large Principal Axis Rotations upon Isotopic Substitution. *J. Phys. Chem. A* **2011**, *115*, 14078–14091.

(19) Laurie, V. W. Note on the Determination of Molecular Structure from Spectroscopic Data. *J. Chem. Phys.* **1958**, *28*, 704–706.

(20) Heo, I.; Lee, J. C.; Özer, B. R.; Schultz, T. Structure of Benzene from Mass-Correlated Rotational Raman Spectroscopy. *RSC Adv.* **2022**, *12*, 21406–21416.

(21) Stanton, J. F. A Refined Estimate of the Bond Length of Methane. *Mol. Phys.* **1999**, *97*, 841–845.

(22) Pawłowski, F.; Jørgensen, P.; Olsen, J.; Hegelund, F.; Helgaker, T.; Gauss, J.; Bak, K. L.; Stanton, J. F. Molecular Equilibrium Structures from Experimental Rotational Constants and Calculated Vibration–Rotation Interaction Constants. *J. Chem. Phys.* **2002**, *116*, 6482–6496.

(23) Becke, A. D. Density-Functional Exchange-Energy Approximation with Correct Asymptotic Behavior. *Phys. Rev. A* **1988**, *38*, 3098.

(24) Lee, C.; Yang, W.; Parr, R. G. Development of the Colle-Salvetti Correlation-Energy Formula into a Functional of the Electron Density. *Phys. Rev. B* **1988**, *37*, 785.

(25) Piccardo, M.; Penocchio, E.; Puzzarini, C.; Biczysko, M.; Barone, V. Semi-Experimental Equilibrium Structure Determinations by Employing B3LYP/SNSD Anharmonic Force Fields: Validation and Application to Semirigid Organic Molecules. *J. Phys. Chem. A* **2015**, *119*, 2058–2082.

(26) Demaison, J.; Craig, N. C.; Cocinero, E. J.; Grabow, J.-U.; Lesarri, A.; Rudolph, H. D. Semiexperimental Equilibrium Structures for the Equatorial Conformers of N-Methylpiperidone and Tropinone by the Mixed Estimation Method. *J. Phys. Chem. A* **2012**, *116*, 8684–8692.

(27) Vogt, N.; Demaison, J.; Cocinero, E. J.; Écija, P.; Lesarri, A.; Rudolph, H. D.; Vogt, J. The Equilibrium Molecular Structures of 2-deoxyribose and Fructose by the Semiexperimental Mixed Estimation Method and Coupled-Cluster Computations. *Phys. Chem. Chem. Phys.* **2016**, *18*, 15555–15563.

(28) Demaison, J.; Vogt, N.; Saragi, R. T.; Juanes, M.; Rudolph, H. D.; Lesarri, A. The S-S Bridge: A Mixed Experimental-Computational Estimation of the Equilibrium Structure of Diphenyl Disulfide. *ChemPhysChem* **2019**, *20*, 366–373.

(29) Lesarri, A.; Mata, S.; López, J. C.; Alonso, J. L. A Laser-Ablation Molecular-Beam Fourier-Transform Microwave Spectrometer: The Rotational Spectrum of Organic Solids. *Rev. Scient. Instrum.* **2003**, *74*, 4799–4804.

(30) Obenchain, D. A.; Spada, L.; Alessandrini, S.; Rampino, S.; Herbers, S.; Tasinato, N.; Mendolicchio, M.; Kraus, P.; Gauss, J.; Puzzarini, C. et al. Unveiling the Sulfur–Sulfur Bridge: Accurate Structural and Energetic Characterization of a Homochalcogen Intermolecular Bond. *Angew. Chem. Int. Ed.* **2018**, *57*, 15822–15826.

(31) McCarthy, M. C.; Cheng, L.; Crabtree, K. N.; Martinez Jr, O.; Nguyen, T. L.; Womack, C. C.; Stanton, J. F. The Simplest Criegee Intermediate (H2C–O–O): Isotopic Spectroscopy, Equilibrium Structure, and Possible Formation from Atmospheric Lightning. *J. Phys. Chem. Lett.* **2013**, *4*, 4133–4139.

(32) Changala, P. B.; Franke, P. R.; Stanton, J. F.; Ellison, G. B.; McCarthy, M. C. Direct Probes of π-Delocalization in Prototypical Resonance-Stabilized Radicals: Hyperfine-Resolved Microwave Spectroscopy of Isotopic Propargyl and Cyanomethyl. *J. Am. Chem. Soc.* **2024**, *146*, 1512–1521.

(33) Penocchio, E.; Piccardo, M.; Barone, V. Semiexperimental Equilibrium Structures for Building Blocks of Organic and Biological Molecules: The B2PLYP Route. *J. Chem. Theory Comp.* **2015**, *11*, 4689–4707.

(34) Penocchio, E.; Mendolicchio, M.; Tasinato, N.; Barone, V. Structural Features of the Carbon–Sulfur Chemical Bond: A Semi-Experimental Perspective. *Can. J. Chem.* **2016**, *94*, 1065–1076.

(35) Stanton, J. F.; Gauss, J.; Christiansen, O. Equilibrium Geometries of Cyclic SiC3 Isomers. *J. Chem. Phys.* **2001**, *114*, 2993–2995.

(36) McCarthy, M. C.; Lattanzi, V.; Kokkin, D.; Martinez Jr, O.; Stanton, J. F. On the Molecular Structure of HOOO. *J. Chem. Phys.* **2012**, *136*, 034303.

(37) McCarthy, M. C.; Lattanzi, V.; Martinez Jr, O.; Gauss, J.; Thorwirth, S. Spectroscopic Detection and Structure of hydroxidooxidosulfur (HOSO) Radical, an Important Intermediate in the Chemistry of Sulfur-Bearing Compounds. *J. Phys. Chem. Lett.* **2013**, *4*, 4074–4079.

(38) Ye, H.; Mendolicchio, M.; Kruse, H.; Puzzarini, C.; Biczysko, M.; Barone, V. The Challenging Equilibrium Structure of HSSH: Another Success of the Rotational Spectroscopy / Quantum Chemistry Synergism. *J. Mol. Struct.* **2020**, *1211*, 127933.

(39) Heim, Z. N.; Amberger, B. K.; Esselman, B. J.; Stanton, J. F.; Woods, R. C.; McMahon, R. J. Molecular Structure Determination: Equilibrium Structure of Pyrimidine from Rotational Spectroscopy (r_e^{SE}) and High-Level Ab Initio Calculation (r_e) Agree Within the Uncertainty of Experimental Measurement. *J. Chem. Phys.* **2020**, *152*, 104303.

(40) Nguyen, H. V. L. The Heavy Atom Substitution and Semi-Experimental Equilibrium Structures of 2-Ethylfuran Obtained by Microwave Spectroscopy. *J. Mol. Struct.* **2020**, *1208*, 127909.

(41) Owen, A. N.; Zdanovskaia, M. A.; Esselman, B. J.; Stanton, J. F.; Woods, R. C.; McMahon, R. J. Semi-Experimental Equilibrium (r_e^{SE}) and Theoretical Structures of Pyridazine (o-$C_4H_4N_2$). *J. Phys. Chem. A* **2021**, *125*, 7976–7987.

(42) Bunn, H. A.; Esselman, B. J.; Franke, P. R.; Kouglas, S. M.; McMahon, R. J.; Stanton, J. F.; Widicious Weaver, S. L.; Woods, R. C. Millimeter/Submillimeter-Wave

Spectroscopy and the Semi- experimental Equilibrium (r_e^{SE}) Structure of 1H-1,2,4-Triazole (c-$C_2H_3N_3$). *J. Phys. Chem. A* **2022**, *126*, 8196–8210.

(43) Ceselin, G.; Salta, Z.; Bloino, J.; Tasinato, N.; Barone, V. Accurate Quantum Chemical Spectroscopic Characterization of Glycolic Acid: A Route toward its Astrophysical Detection. *J. Phys. Chem. A* **2022**, *126*, 2373–2387.

(44) Smith, H. H.; Esselman, B. J.; Wood, S. A.; Stanton, J. F.; Woods, R. C.; McMahon, R. J. Improved Semi-Experimental Equilibrium Structure and High-Level Theoretical Structures of Ketene. *J. Chem. Phys.* **2023**, *158*, 244304.

(45) Barone, V.; Ceselin, G.; Lazzari, F.; Tasinato, N. Toward Spectroscopic Accuracy for the Structures of Large Molecules at DFT Cost: Refinement and Extension of the Nano-LEGO Approach. *J. Phys. Chem. A* **2023**, *127*, 5183–5192.

(46) Li, X.; Spada, L.; Alessandrini, S.; Zheng, Y.; Lengsfeld, K. G.; Grabow, J.-U.; Feng, G.; Puzzarini, C.; Barone, V. Stacked but not Stuck: Unveiling the Role of $\pi \leftarrow \pi*$ Interactions with the Help of the Benzofuran–Formaldehyde Complex. *Angew. Chem. Int. Ed.* **2022**, *61*, e202113737.

(47) Pietropolli Charmet, A.; Stoppa, P.; De Lorenzi, A.; Melosso, M.; Achilli, A.; Dore, L.; Puzzarini, C.; Canè, E.; Tamassia, F. Computational, Rotational and Ro-Vibrational Experimental Investigation of Monodeuterated Chloromethane. *J. Quantit. Spectrosc. Radiat. Transfer* **2023**, *305*, 108624.

(48) Jiang, N.; Melosso, M.; Alessandrini, S.; Bizzocchi, L.; Martin-Drumel, M.-A.; Pirali, O.; Puzzarini, C. Insights into the Molecular Structure and Infrared Spectrum of the Prebiotic Species Aminoacetonitrile. *Phys. Chem. Chem. Phys.* **2023**, *25*, 4754–4763.

(49) Melosso, M.; Alessandrini, S.; Spada, L.; Melli, A.; Wang, X.; Zheng, Y.; Duan, C.;

Li, J.; Du, W.; Gou, Q. et al. Rotational Spectra and Semi-Experimental Structures of Furonitrile and Its Water Cluster. *Phys. Chem. Chem. Phys.* **2023**, *25*, 31281–31291.

(50) Ceselin, G.; Barone, V.; Tasinato, N. Accurate Biomolecular Structures by the Nano-LEGO Approach: Pick the Bricks and Build Your Geometry. *J. Chem. Theory Comput.* **2021**, *17*, 7290–7311.

(51) Jensen, F. *Introduction to Computational Chemistry*; John Wiley & Sons, 2017.

(52) Krylov, A. I. The Quantum Chemistry of Open-Shell Species. *Rev. Comput. Chem.* **2017**, *30*, 151–224.

(53) Glaesemann, K. R.; Schmidt, M. W. On the Ordering of Orbital Energies in High-Spin ROHF. *J. Phys. Chem. A* **2010**, *114*, 8772–8777.

(54) Watts, J. D.; Gauss, J.; Bartlett, R. J. Coupled-Cluster Methods with Noniterative Triple Excitations for Restricted Open-Shell Hartree–Fock and Other General Single Determinant Reference Functions. Energies and Analytical Gradients. *J. Chem. Phys.* **1993**, *98*, 8718–8733.

(55) Menon, A. S.; Radom, L. Consequences of Spin Contamination in Unrestricted Calculations on Open-Shell Species: Effect of Hartree Fock and Møller Plesset Contributions in Hybrid and Double-Hybrid Density Functional Theory Approaches. *J. Phys. Chem. A* **2008**, *112*, 13225–13230.

(56) Møller, C.; Plesset, M. S. Note on an Approximation Treatment for Many-Electron Systems. *Phys. Rev.* **1934**, *46*, 618.

(57) Purvis III, G. D.; Sekino, H.; J., B. R. Multiplicity of Many-Body Wavefunctions using Unrestricted Hartree-Fock Reference Functions. *Collect. Czech. Chem. Commun.* **1988**, *53*, 2203–2213.

(58) Santra, G.; Sylvetsky, N.; Martin, J. M. Minimally empirical double-hybrid functionals trained against the GMTKN55 database: revDSD-PBEP86-D4, revDOD-PBE-D4, and DOD-SCAN-D4. *J. Phys. Chem. A* **2019**, *123*, 5129–5143.

(59) Barone, V.; Lupi, J.; Salta, Z.; Tasinato, N. Development and Validation of a Parameter-Free Model Chemistry for the Computation of Reliable Reaction Rates. *J. Chem. Theory Comput.* **2021**, *17*, 4913–4928.

(60) Cernicharo, J.; Guélin, M.; Agúndez, M.; McCarthy, M. C.; Thaddeus, P. Detection of C_5N^- and Vibrationally Excited C_6H in IRC+10216. *Astrophys. J.* **2008**, *688*, L83–L86.

(61) Puzzarini, C.; Barone, V. Toward Spectroscopic Accuracy for Organic Free Radicals: Molecular Structure, Vibrational Spectrum, and Magnetic Properties of F_2NO. *J. Chem. Phys.* **2008**, *129*, 084306.

(62) Puzzarini, C.; Barone, V. Toward Spectroscopic Accuracy for Open-Shell Systems: Molecular Structure and Hyperfine Coupling Constants of H_2CN, H_2CP, NH_2, and PH_2 as test cases. *J. Chem Phys.* **2010**, *133*.

(63) Nikow, M.; Wilhelm, M. J.; Dai, H.-L. Vibrational Modes of the Vinyl and Deuterated Vinyl Radicals. *J. Phys. Chem. A* **2009**, *113*, 8857–8870.

(64) Changala, P. B.; McCarthy, M. C. Hyperfine-Resolved Rotational Spectroscopy of Phenyl Radical. *J. Phys. Chem. Lett.* **2023**, *14*, 5370–5376.

(65) Melli, A.; Tonolo, F.; Barone, V.; Puzzarini, C. Extending the Applicability of the Semi-Experimental Approach by means of "Template Molecule" and "Linear Regression" Models on top of DFT Computations. *J. Phys. Chem. A* **2021**, *125*, 9904–9916.

(66) Ye, H.; Alessandrini, S.; Melosso, M.; Puzzarini, C. Exploiting the "Lego brick" ap-

proach to predict accurate molecular structures of PAHs and PANHs. *Phys. Chem. Chem. Phys.* **2022**, *24*, 23254–23264.

(67) Martinez Jr, O.; Crabtree, K. N.; Gottlieb, C. A.; Stanton, J. F.; McCarthy, M. C. An Accurate Molecular Structure of Phenyl, the Simplest Aryl Radical. *Angew. Chem. Int. Ed.* **2015**, *127*, 1828–1831.

(68) Johansen, S. L.; Martin-Drumel, M.-A.; Crabtree, K. N. Rotational Spectrum of the β-Cyanovinyl Radical: A Possible Astrophysical N-Heterocycle Precursor. *J. Phys. Chem. A* **2019**, *123*, 5171–5177.

(69) Cabezas, C.; Chang, C.-H.; Guillemin, J.-C.; Endo, Y. Gas-Phase Spectroscopic Identification of the Chlorovinyl Radical. *Phys. Chem. Chem. Phys.* **2022**, *24*, 25099–25105.

(70) Liu, Y.-T.; Chang, C.-H.; Nakajima, M.; Endo, Y. Fourier-transform microwave spectroscopy of the s-trans-3-propenalyl (CH2CHĊO) and 3-propenolyl (ĊH2CHCO) radicals. *Phys. Chem. Chem. Phys.* **2023**, *25*, 33112–33118.

(71) Gordon, V. D.; McCarthy, M.; Apponi, A.; Thaddeus, P. Rotational Spectra of Sulfur-Carbon Chains. I. The Radicals C_4S, C_5S, C_6S, C_7S, C_8S, and C_9S. *Astrophys J. Suppl. S.* **2001**, *134*, 311.

(72) Stanton, J. F.; Gauss, J.; Cheng, L.; Harding, M. E.; Matthews, D. A.; Szalay, P. G. CFOUR, Coupled-Cluster techniques for Computational Chemistry, a quantum-chemical program package. With contributions from A.A. Auer, R.J. Bartlett, U. Benedikt, C. Berger, D.E. Bernholdt, Y.J. Bomble, O. Christiansen, F. Engel, R. Faber, M. Heckert, O. Heun, M. Hilgenberg, C. Huber, T.-C. Jagau, D. Jonsson, J. Jusélius, T. Kirsch, K. Klein, W.J. Lauderdale, F. Lipparini, T. Metzroth, L.A. Mück, D.P. O'Neill, D.R. Price, E. Prochnow, C. Puzzarini, K. Ruud, F. Schiffmann, W. Schwalbach, C. Simmons, S. Stopkowicz, A. Tajti, J. Vázquez, F. Wang, J.D. Watts and the integral packages MOLECULE (J. Almlöf and P.R. Taylor), PROPS

(P.R. Taylor), ABACUS (T. Helgaker, H.J. Aa. Jensen, P. Jørgensen, and J. Olsen), and ECP routines by A. V. Mitin and C. van Wüllen. For the current version, see http://www.cfour.de.

(73) Matthews, D. A.; Cheng, L.; Harding, M. E.; Lipparini, F.; Stopkowicz, S.; Jagau, T.-C.; Szalay, P. G.; Gauss, J.; Stanton, J. F. Coupled-Cluster Techniques for Computational Chemistry: The CFOUR Program Package. *J. Chem. Phys.* **2020**, *152*, 214108.

(74) Aliev, M. R.; Watson, J. K. G. Higher-Order Effects in the Vibration–Rotation Spectra of Semirigid Molecules. In *Molecular Spectroscopy: Modern Research*; Rao, K. N., Ed.; Academic Press, 1985; Vol. 3; pp 1–67.

(75) Frisch, M. J.; Trucks, G. W.; Schlegel, H. B.; Scuseria, G. E.; Robb, M. A.; Cheeseman, J. R.; Scalmani, G.; Barone, V.; Petersson, G. A.; Nakatsuji, H. et al. Gaussian16 Revision C.01. 2016; Gaussian Inc. Wallingford CT.

(76) Raghavachari, K.; Trucks, G. W.; Pople, J. A.; Head-Gordon, M. A Fifth-Order Perturbation Comparison of Electron Correlation Theories. *Chem. Phys. Lett.* **1989**, *157*, 479–483.

(77) Mendolicchio, M.; Barone, V. Unbiased Comparison between Theoretical and Experimental Molecular Structures and Properties: Toward an Accurate Reduced-Cost Evaluation of Vibrational Contributions. *J. Chem. Theory Comput.* **2024**, *20*, 2842–2857.

(78) Uribe, L.; Di Grande, S.; Crisci, L.; Lazzari, F.; Mendolicchio, M.; Barone, V. Accurate Structures and Rotational Constants of Steroid Hormones at DFT Cost: Androsterone, Testosterone, Estrone, β-Estradiol, and Estriol. *J. Phys. Chem. A* **2024**, *128*, 2629–2642.

(79) Flygare, W. H. Magnetic Interactions in Molecules and an Analysis of Molecular Electronic Charge Distribution from Magnetic Parameters. *Chem. Rev.* **1974**, *74*, 653–.687.

(80) Gauss, J.; Ruud, K.; Kállay, M. Gauge-Origin Independent Calculation of Magnetizabilities and Rotational g Tensors at the Coupled-Cluster Level. *J. Chem. Phys.* **2007**, *127*, 074101.

(81) Dunning Jr, T. H. Gaussian Basis Sets for Use in Correlated Molecular Calculations. I. The Atoms Boron through Neon and Hydrogen. *J. Chem. Phys.* **1989**, *90*, 1007–1023.

(82) Kendall, A.; Dunning Jr., T. H.; Harrison, R. J. Electron Affinities of the First-Row Atoms Revisited. Systematic Basis Sets and Wave Functions. *J. Chem. Phys.* **1992**, *96*, 6796.

(83) Woon, D. E.; Dunning Jr, T. H. Gaussian Basis Sets for Use in Correlated Molecular Calculations. III. The Atoms Aluminum through Argon. *J. Chem. Phys.* **1993**, *98*, 1358–1371.

(84) Martin-Drumel, M. A.; Pirali, O.; Balcon, D.; Bréchignac, P.; Roy, P.; Vervloet, M. High Resolution Far-Infrared Fourier Transform Spectroscopy of Radicals at the AILES Beamline of SOLEIL Synchrotron Facility. *Rev. Sci. Instrum.* **2011**, *82*, 113106.

(85) Tanimoto, M.; Saito, S.; Hirota, E. Microwave Spectrum of the Boron Monoxide Radical, BO. *J. Chem. Phys.* **1986**, *84*, 1210–1214.

(86) McCarthy, M. C.; Mohamed, S.; Brown, J. M.; Thaddeus, P. Detection of Low-Frequency Lambda-Doublet Transitions of the free ^{12}CH and ^{13}CH radicals. *Proc. Natl. Acad. Sci. USA* **2006**, *103*, 12263–12268.

(87) Martin-Drumel, M.; Eliet, S.; Pirali, O.; Guinet, M.; Hindle, F.; Mouret, G.; Cuis-

set, A. New Investigation on THz Spectra of OH and SH Radicals ($X^2\Pi_i$). *Chem. Phys. Lett.* **2012**, *550*, 8–14.

(88) Müller, H. S.; Kobayashi, K.; Takahashi, K.; Tomaru, K.; Matsushima, F. Terahertz Spectroscopy of $N^{18}O$ and Isotopic Invariant Fit of Several Nitric Oxide Isotopologs. *J. Mol. SpectrOSC.* **2015**, *310*, 92–98.

(89) Abrams, M. C.; Davis, S. P.; Rao, M.; Engleman, R. High-Resolution Fourier Transform Spectroscopy of the Vibration-Rotation Spectrum of the OD Radical. *J. Mol. Spectrosc.* **1994**, *165*, 57–74.

(90) Saleck, A. H.; Yamada, K. M. T.; Winnewisser, G. Isotopic Nitric Oxide Spectra and Breakdown of the Born-Oppenheimer Approximation. *Mol. Phys.* **1991**, *72*, 1135–1148.

(91) Drouin, B. J. Isotopic Spectra of the Hydroxyl Radical. *J. Phys. Chem. A* **2013**, *117*, 10076–10091.

(92) Saleck, A. H.; Liedtke, M.; Dolgner, A.; Winnewisser, G. Rotational Spectra of $^{14}N^{17}O$ and $^{15}N^{18}O$. *Z. Naturforsch. A* **1994**, *49*, 1111–1118.

(93) Morino, I.; Takagi, K.; Kawaguchi, K. Fourier Transform Emission Spectroscopy of the $\Delta v = 1$ Bands of the ^{18}OH Radical. *Mol. Phys.* **2007**, *105*, 841–848.

(94) Klisch, E.; Klaus, T.; Belov, S.; Dolgner, A.; Schieder, R.; Winnewisser, G.; Herbst, E. The Rotational Spectrum of SH and SD. *Astrophys. J.* **1996**, *473*, 1118.

(95) Lattanzi, V.; Cazzoli, G.; Puzzarini, C. Rare Isotopic Species of Sulfur Monoxide: The Rotational Spectrum in the THz Region. *Astrophys. J.* **2015**, *813*, 4.

(96) Lewen, F.; Brünken, S.; Winnewisser, G.; Šimečková, M.; Urban, Š. Doppler-Limited Rotational Spectrum of the NH Radical in the 2 THz Region. *J. Mol. Spectrosc.* **2004**, *226*, 113–122.

(97) Klaus, T.; Saleck, A.; Belov, S.; Winnewisser, G.; Hirahara, Y.; Hayashi, M.; Kagi, E.; Kawaguchi, K. Pure rotational spectra of SO: Rare isotopomers in the 80-GHz to 1.1-THz region. *J. Mol. SpectrOSC.* **1996**, *180*, 197–206.

(98) Dore, L.; Bizzocchi, L.; Degli Esposti, C.; Tamassia, F. Fine and Hyperfine Structure of the Transition of ND ($X^3\Sigma^-$) in Vibrational Excited States. *Mol. Phys.* **2011**, *109*, 2191–2198.

(99) Bizzocchi, L.; Melosso, M.; Dore, L.; Degli Esposti, C.; Tamassia, F.; Prudenzano, D.; Lattanzi, V.; Laas, J.; Spezzano, S.; Giuliano, B. M. et al. Accurate Laboratory Measurement of the Complete Fine Structure of the $N = 1 - 0$ Transition of ^{15}NH. *Astrophys. J.* **2018**, *863*, 3.

(100) Melosso, M.; Bizzocchi, L.; Tamassia, F.; Degli Esposti, C.; Canè, E.; Dore, L. The Rotational Spectrum of ^{15}ND. Isotopic-Independent Dunham-Type Analysis of the Imidogen Radical. *Phys. Chem. Chem. Phys.* **2019**, *21*, 3564–3573.

(101) Klisch, E.; Klein, H.; Winnewisser, G.; Herbst, E. Laboratory Rotational Spectrum of PH ($N = 2 \leftarrow 1$) in the 1 THz Region. *Z. Naturforsch. A* **1998**, *53*, 733–742.

(102) Goto, M.; Saito, S. Submillimeter-Wave Spectra of the PH and PD Radicals in the $^3\Sigma^-$ state. *Chem. Phys. Lett.* **1993**, *211*, 443–448.

(103) Lee, S. K.; Ozeki, H.; Saito, S. Microwave Spectrum of the NS Radical in the $^2\Pi_r$ Ground Electronic State. *Astrophys. J., Suppl. S.* **1995**, *98*, 351.

(104) Fujiwara, H.; Kobayashi, K.; Ozeki, H.; Saito, S.; Jaman, A. I. Submillimetre-Wave Spectra of AsH and AsD Radicals in the $X^3\Sigma^-$ Electronic State. *J. Chem. Soc. Faraday Trans.* **1997**, *93*, 1045–1051.

(105) Saleck, A. H.; Ozeki, H.; Saito, S. Isotopic NS Rotational Spectra: ^{14}N^{33}S and ^{15}N^{32}S. *Chem. Phys. Lett.* **1995**, *244*, 199–206.

(106) Hübner, M.; Castillo, M.; Davies, P.; Röpcke, J. Diode laser spectroscopy of the fundamental bands of $^{12}C^{14}N$, $^{13}C^{14}N$, $^{12}C^{15}N$, $^{13}C^{15}N$ free radicals in the ground $^2\Sigma^+$ electronic state. *Spectrochim. Acta A Mol. Biomol. Spectrosc.* **2005**, *61*, 57–60.

(107) Saleck, A.; Simon, R.; Winnewisser, G. Interstellar CN Rotational Spectra: $^{12}C^{15}N$. *Astrophys. J.* **1994**, *436*, 176–182.

(108) Bogey, M.; Demuynck, C.; Destombes, J. The Millimetre Wave Spectrum of the $^{13}C^{14}N$ Radical in Its Ground State. *Can. J. Phys.* **1984**, *62*, 1248–1253.

(109) Hübner, M.; Castillo, M.; Davies, P.; Röpcke, J. Diode Laser Spectroscopy of the Fundamental Bands of $^{12}C^{14}N$, $^{13}C^{14}N$, $^{12}C^{15}N$, $^{13}C^{15}N$ Free Radicals in the Ground $^2\Sigma^+$ Electronic State. *Spectrochim. Acta A* **2005**, *61*, 57–60.

(110) Ozeki, H.; Saito, S. Laboratory Submillimeter-Wave Spectroscopy of the CH_2 ($^3B_1$) radical. *Astrophys. J. Lett.* **1995**, *451*, L97.

(111) McCarthy, M.; Tamassia, F.; Woon, D. E.; Thaddeus, P. A Laboratory and Theoretical Study of Silicon Hydroxide SiOH. *J. Chem. Phys.* **2008**, *129*, 184301.

(112) Ozeki, H.; Bailleux, S.; Wlodarczak, G. Terahertz Spectroscopy of the CHD Radical (Σ^3A''). *Astron. Astrophys.* **2011**, *527*, A64.

(113) Martin-Drumel, M.; Pirali, O.; Vervloet, M. Synchrotron Based FT-FIR Pure Rotational Spectroscopy of the NH_2 Radical in Its Two Lowest Vibrational States. *J. Phys. Chem. A* **2014**, *118*, 1331–1338.

(114) Bizzocchi, L.; Melosso, M.; Giuliano, B. M.; Dore, L.; Tamassia, F.; Martin-Drumel, M.-A.; Pirali, O.; Margulès, L.; Caselli, P. Submillimeter and Far-infrared Spectroscopy of Monodeuterated Amidogen Radical (NHD): Improved Rest Frequencies for Astrophysical Observations. *Astrophys. J. Suppl. S.* **2020**, *247*, 59.

(115) Margulès, L.; Martin-Drumel, M.; Pirali, O.; Bailleux, S.; Wlodarczak, G.; Roy, P.; Roueff, E.; Gerin, M. Terahertz Spectroscopy of the $^{15}NH_2$ Amidogen Radical. *Astron. Astrophys.* **2016**, *591*, A110.

(116) Habara, H.; Yamamoto, S.; Amano, T. Submillimeter-Wave Spectra of HCS and DCS. *J. Chem. Phys.* **2002**, *116*, 9232–9238.

(117) Melosso, M.; Dore, L.; Degli Esposti, C.; Tamassia, F.; Cané, E.; Bizzocchi, L. Terahertz Spectroscopy of Isotopologues of Amidogen Radical. The 25th International Conference on High Resolution Molecular Spectroscopy. 2018.

(118) Melosso, M.; Degli Esposti, C.; Dore, L. Terahertz Spectroscopy and Global Analysis of the Rotational Spectrum of Doubly Deuterated Amidogen Radical ND_2. *Astrophys. J. Suppl. S.* **2017**, *233*, 15.

(119) Habara, H.; Yamamoto, S. The ^{13}C Hyperfine Constants of HCS and HSC Studied by Microwave Spectroscopy. *J. Mol. Spectrosc.* **2003**, *219*, 30–36.

(120) Melosso, M.; Conversazioni, B.; Degli Esposti, C.; Dore, L.; Cané, E.; Tamassia, F.; Bizzocchi, L. The Pure Rotational Spectrum of $^{15}ND_2$ Observed by Millimetre and Submillimetre-Wave Spectroscopy. *J. Quant. Spectrosc. Radiat. Transfer* **2019**, *222*, 186–189.

(121) Habara, H.; Yamamoto, S. Microwave Spectrum and Molecular Structure of the HSC Radical. *J. Chem. Phys.* **2000**, *112*, 10905–10911.

(122) Margulès, L.; Herbst, E.; Ahrens, V.; Lewen, F.; Winnewisser, G.; Müller, H. The Phosphidogen Radical, PH_2: Terahertz Spectrum and Detectability in Space. *J. Mol. Spectrosc.* **2002**, *211*, 211–220.

(123) Furuya, T.; Saito, S. Microwave Spectrum of PHD: Hyperfine Structure. *J. Mol. Spectrosc.* **2003**, *220*, 122–131.

(124) Hirao, T.; Hayakashi, S.-i.; Yamamoto, S.; Saito, S. Microwave Spectrum of the PD_2 Radical in the $^2B_1$ Ground Electronic State. *J. Mol. Spectrosc.* **1998**, *187*, 153–162.

(125) Cazzoli, G.; Lattanzi, V.; Kirsch, T.; Gauss, J.; Tercero, B.; Cernicharo, J.; Puzzarini, C. Laboratory Measurements and Astronomical Search for the HSO Radical. *Astron. Astrophys.* **2016**, *591*, A126.

(126) Fujiwara, H.; Kobayashi, K.; Ozeki, H.; Saito, S. Submillimeter-Wave Spectrum of the AsH_2 Radical in the $^2B_1$ Ground Electronic State. *J. Chem. Phys.* **1998**, *109*, 5351–5355.

(127) Endo, Y.; Saito, S.; Hirota, E. Microwave Spectra of the HSO and DSO Radicals. *J. Chem. Phys.* **1981**, *75*, 4379–4384.

(128) Fujiwara, H.; Saito, S. Microwave Spectrum of the AsD_2 ($^2B_1$) Radical: Harmonic Force Field and Molecular Structure. *J. Mol. Spectrosc.* **1998**, *192*, 399–405.

(129) Puzzarini, C.; Alessandrini, S.; Bizzocchi, L.; Melosso, M. Hunting for Interstellar Molecules: Rotational Spectra of Reactive Species. *Faraday Discuss.* **2023**, *245*, 309–326.

(130) Blake, G. A.; Sastry, K.; De Lucia, F. C. The Laboratory Millimeter and Submillimeter Spectrum of HCO. *J. Chem. Phys.* **1984**, *80*, 95–101.

(131) Yamamoto, S.; Saito, S.; Kawaguchi, K.; Chikada, Y.; Suzuki, H.; Kaifu, N.; Ishikawa, S.-I.; Ohishi, M. Rotational Spectrum of the CCS Radical Studied by Laboratory Microwave Spectroscopy and Radio-Astronomical Observations. *Astrophys. J.* **1990**, *361*, 318–324.

(132) Endo, Y.; Hirota, E. The Millimeter-and Submillimeter-Wave Spectrum of the DCO Radical. *J. Mol. Spectrosc.* **1988**, *127*, 540–545.

(133) Ikeda, M.; Sekimoto, Y.; Yamamoto, S. Fourier Transform Microwave Spectroscopy of ^{13}C-Substituted CCS Radicals. *J. Mol. Spectrosc.* **1997**, *185*, 21–25.

(134) Kolesniková, L.; Varga, J.; Beckers, H.; Šimečková, M.; Zelinger, Z.; Stříteská, L. N.; Kania, P.; Willner, H.; Urban, Š. Detailed Study of Fine and Hyperfine Structures in Rotational Spectra of the Free Fluoroformyloxyl Radical $FCO_2\cdot$ *J. Chem. Phys.* **2008**, *128*, 224302.

(135) Suma, K.; Sumiyoshi, Y.; Endo, Y. The Rotational Spectrum and Structure of the HOOO Radical. *Science* **2005**, *308*, 1885–1886.

(136) Kouckỳ, J.; Kania, P.; Uhlikova, T.; Kolesniková, L.; Beckers, H.; Willner, H.; Urban, Š. Geometry and Microwave Rotational Spectrum of the $FC^{16}O^{18}O$ Radical. *J. Phys. Chem. A* **2013**, *117*, 10138–10143.

(137) Kouckỳ, J.; Kolesniková, L.; Uhlíková, T.; Varga, J.; Kania, P.; Beckers, H.; Willner, H.; Urban, Š. The Fluoroformyloxyl Radical Geometry and Ground-State Rotational Spectra of the Free $FC^{18}O_2$ Radical. *J. Chem. Phys.* **2012**, *136*, 094309.

(138) Endo, Y.; Saito, S.; Hirota, E. The microwave spectrum of the chloromethyl radical, CH_2Cl. *Can. J. Phys.* **1984**, *62*, 1347–1360.

(139) Barreau, L.; Martinez Jr, O.; Crabtree, K. N.; Womack, C. C.; Stanton, J. F.; McCarthy, M. C. Oxygen-18 Isotopic Studies of HOOO and DOOO. *J. Phys. Chem. A* **2017**, *121*, 6296–6303.

(140) McCarthy, M. C.; Martinez Jr, O.; McGuire, B. A.; Crabtree, K. N.; Martin-Drumel, M.-A.; Stanton, J. F. Isotopic Studies of *trans*- and *cis*-HOCO Using Rotational Spectroscopy: Formation, Chemical Bonding, and Molecular Structures. *J. Chem. Phys.* **2016**, *144*, 124304.

(141) Puzzarini, C. Molecular Structure of Thiourea. *J. Phys. Chem. A* **2012**, *116*, 4381–4387.

(142) Cabezas, C.; Peña, I.; Cernicharo, J. Laboratory Rotational Spectroscopy and Astronomical Search of Ethynyl Substituted Naphthalene. *Mon. Not. R. Astron. Soc* **2023**, *519*, 2590–2597.

(143) Spaniol, J.-T.; Lee, K. L. K.; Pirali, O.; Puzzarini, C.; Martin-Drumel, M.-A. A Rotational Investigation of the Three Isomeric Forms of Cyanoethynylbenzene (HCC-C_6H_4-CN): Benchmarking Experiments and Calculations using the "Lego brick" Approach. *Phys. Chem. Chem. Phys.* **2023**, *25*, 6397–6405.

(144) Dunning Jr, T. H.; Peterson, K. A.; Wilson, A. K. Gaussian Basis Sets for Use in Correlated Molecular Calculations. X. The Atoms Aluminum Through Argon Revisited. *J. Chem. Phys.* **2001**, *114*, 9244–9253.

(145) Papajak, E.; Truhlar, D. G. Convergent Partially Augmented Basis Sets for Post-Hartree-Fock Calculations of Molecular Properties and Reaction Barrier Heights. *J. Chem. Theory Comput.* **2011**, *7*, 10–18.

(146) Goerigk, L.; Grimme, S. Efficient and Accurate Double-Hybrid-Meta-GGA Density Functionals Evaluation with the Extended GMTKN30 Database for General Main Group Thermochemistry, Kinetics, and Noncovalent Interactions. *J. Chem. Theory Comput.* **2011**, *7*, 291–309.

(147) Grimme, S.; Ehrlich, S.; Goerigk, L. Effect of the Damping Function in Dispersion Corrected Density Functional Theory. *J. Chem. Theory Comput.* **2011**, *32*, 1456–1465.

(148) Demaison, J.; Møllendal, H.; Perrin, A.; Orphal, J.; Tchana, F. K.; Rudolph, H.; Willaert, F. Microwave and high resolution infrared spectra of vinyl chloride, ab initio

anharmonic force field and equilibrium structure. *J. Mol. Spectrosc.* **2005**, *232*, 174–185.

(149) Botschwina, P. Spectroscopic Properties of Interstellar Molecules: Theory and Experiment. *Phys. Chem. Chem. Phys.* **2003**, *5*, 3337–3348.

(150) Bogey, M.; Civiš, S.; Delcroix, B.; Demuynck, C.; Krupnov, A.; Quiguer, J.; Tretyakov, M.; Walters, A. Microwave Spectrum up to 900 GHz of SO Created in Highly Excited States by Electric Discharge and UV-Laser Photolysis. *J. Mol. Spectr.* **1997**, *182*, 85–97.

(151) Osiac, M.; Röpcke, J.; Davies, P. Infrared Laser Spectrum of the Fundamental Band of the Boron Monoxide Free Radical. *Chem. Phys. LetT.* **2001**, *344*, 92–96.

(152) Bernath, P. F. The Vibration–Rotation Emission Spectrum of CH($X^2\Pi$). *J. Chem. Phys.* **1987**, *86*, 4838–4842.

(153) Dane, C. B.; Lander, D.; Curl, R.; Tittel, F.; Guo, Y.; Ochsner, M. I.; Moore, C. B. Infrared Flash Kinetic Spectroscopy of HCO. *J. Chem. Phys.* **1988**, *88*, 2121–2128.

(154) McKellar, A.; Vervloet, M.; Burkholder, J. B.; Howard, C. J. A Combined Analysis of the ν_1, ν_3, and $2\nu_2$ Vibrational States of the NH_2 Radical Using Fourier Transform Absorption and Emission Data. *J. Mol. Spectr.* **1990**, *142*, 319–335.

(155) Grimme, S. Semiempirical Hybrid Density Functional with Perturbative Second-Order Correlation. *J. Chem. Phys.* **2006**, *124*, 034108.

(156) Demaison, J.; Margulès, L.; Boggs, J. E. Equilibrium Structure and Force Field of NH_2. *Phys. Chem. Chem. Phys.* **2003**, *5*, 3359–3363.

(157) Franke, P. R.; Stanton, J. F. Influence of Fourth-Order Vibrational Corrections on Semi-Experimental (r_e^{SE}) Structures of Linear Molecules. *J. Chem. Phys.* **2024**, *160*.

(158) Ram, R.; Bernath, P. Fourier Transform Infrared Emission Spectroscopy of ND and PH. *J. Mol. Spectrosc.* **1996**, *176*, 329–336.

(159) Saleck, A. H.; Simon, R.; Winnewisser, G. Interstellar CN Rotational Spectra: $^{12}C^{15}N$. *Astrophys. J* **1994**, *436*, 176.

(160) Thorpe, J. H.; Feller, D.; Bross, D. H.; Ruscic, B.; Stanton, J. F. Sub 20 cm^{-1} Computational Prediction of the CH Bond Energy–A case of Systematic Error in Computational Thermochemistry. *Phys. Chem. Chem. Phys.* **2023**, *25*, 21162–21172.

(161) Matsumura, K.; Kawaguchi, K.; Nagai, K.; Yamada, C.; Hirota, E. Infrared Diode Laser Spectroscopy of the NS Radical. *J. Mol. Spectrosc.* **1980**, *84*, 68–73.

(162) Puzzarini, C.; Gauss, J. Quantum-Chemical Determination of Born–Oppenheimer Breakdown Parameters for Rotational Constants: The Open-Shell Species CN, CO^+ and BO. *Mol. Phys.* **2013**, *111*, 2204–2210.

(163) Thorpe, J. H.; Lopez, C. A.; Nguyen, T. L.; Baraban, J. H.; Bross, D. H.; Ruscic, B.; Stanton, J. F. High-Accuracy Extrapolated Ab Initio Thermochemistry. IV. A Modified Recipe for Computational Efficiency. *J. Chem. Phys.* **2019**, *150*, 224102.

(164) Vermeeren, P.; Bickelhaupt, F. M. The abnormally long and weak methylidyne C–H bond. *Nat. Sci.* **2023**, *3*, e20220039.

(165) Agúndez, M.; Marcelino, N.; Cernicharo, J.; Tafalla, M. Detection of Interstellar HCS and Its Metastable Isomer HSC: New Pieces in the Puzzle of Sulfur Chemistry. *Astron. Astrophys.* **2018**, *611*, L1.

(166) Puzzarini, C. The HCS/HSC and HCS^+/HSC^+ Systems: Molecular Properties, Isomerization, and Energetics. *J. Chem. Phys.* **2005**, *123*, 024313.

(167) Ma, B.; Allinger, N. L. Calculation of r_z Structures from r_s Structures. *J. Mol. Struct.* **1997**, *413-414*, 395–404.

(168) Alessandrini, S.; Gauss, J.; Puzzarini, C. Accuracy of Rotational Parameters Predicted by High-Level Quantum-Chemical Calculations: Case Study of Sulfur-Containing Molecules of Astrochemical Interest. *J. Chem. Theory Comput.* **2018**, *14*, 5360–5371.

(169) Marcelino, N.; Puzzarini, C.; Agúndez, M.; Fuentetaja, R.; Tercero, B.; de Vicente, P.; Cernicharo, J. First Detection of the HSO Radical in Space. *Astron. Astrophys.* **2023**, *674*, L13.

(170) Koput, J. Equilibrium Structure and Vibrational-Rotational Energy Levels of the X^2A' SiOH/HSiO Radical System. *J. Phys. Chem. A* **2002**, *106*, 12067–12071.

(171) Egorov, O.; Rey, M.; Viglaska, D.; Nikitin, A. V. Accurate Ab Initio Potential Energy Surface, Rovibrational Energy Levels and Resonance Interactions of Triplet ($\tilde{X}^3B_1$) Methylene. *J. Comput. Chem.* **2024**, *45*, 83–100.

(172) Kobayashi, K.; Ozeki, H.; Saito, S.; Tonooka, M.; Yamamoto, S. The Microwave Spectrum of the NHD Radical in the Ground Electronic State, $^2A''$. *J. Chem. Phys.* **1997**, *107*, 9289–9296.

(173) Francisco, J. S.; Muckerman, J. T.; Yu, H.-G. HOCO Radical Chemistry. *Acc. Chem. Res.* **2010**, *43*, 1519–1526.

(174) Bartlett, M. A.; Kazez, A. H.; Schaefer, H. F.; Allen, W. D. Riddles of the Structure and Vibrational Dynamics of HO_3 Resolved Near the Ab Initio Limit. *J. Chem. Phys.* **2019**, *151*, 094304.

(175) East, A. L.; Allen, W. D. The Heat of Formation of NCO. *J. Chem. Phys.* **1993**, *99*, 4638–4650.

(176) Császár, A. G.; Allen, W. D.; Schaefer III, H. F. In Pursuit of the Ab Initio Limit for Conformational Energy Prototypes. *J. Chem. Phys.* **1998**, *108*, 9751–9764.

(177) Suma, K.; Sumiyoshi, Y.; Endo, Y. Force-Field Calculation and Geometry of the HOOO Radical. *J. Chem. Phys.* **2013**, *139*, 094301.

(178) Cabezas, C.; Chang, C.-H.; Guillemin, J.-C.; Endo, Y. Gas-Phase Spectroscopic Identification of the Chlorovinyl Radical. *Phys. Chem. Chem. Phys.* **2022**, *24*, 25099–25105.

(179) Liu, Y.-T.; Chang, C.-H.; Nakajima, M.; Endo, Y. Fourier-Transform Microwave Spectroscopy of the s-trans-3-Propenalyl (CH_2CHCO) and 3-Propenolyl (CH_2CHCO) Radicals. *Phys. Chem. Chem. Phys.* **2023**, *25*, 33112–33118.

(180) Barone, V.; Lazzari, F. Hunting for Complex Organic Molecules in the Interstellar Medium: the Role of Accurate Low-Cost Theoretical Geometries and Rotational Constants. *J. Phys. Chem. A* **2023**, *127*, 10517–10527.

(181) Barone, V. Quantum Chemistry Meets High-Resolution Spectroscopy for Characterizing the Molecular Bricks of Life in the Gas-Phase. *Phys. Chem. Chem. Phys.* **2024**, *26*, 5802—-5821.

(182) Szalay, P. G.; Thøgersen, L. S.; Olsen, J.; Kállay, M.; Gauss, J. Equilibrium Geometry of the Ethynyl (CCH) Radical. *J. Phys. Chem. A* **2004**, *108*, 3030–3034.

(183) Puzzarini, C.; Heckert, M.; Gauss, J. The Accuracy of Rotational Constants Predicted by High-Level Quantum-Chemical Calculations. I. Molecules Containing First-Row Atoms. *J. Chem. Phys.* **2008**, *128*, 194108.

(184) Jochnowitz, E. B.; Zhang, X.; Nimlos, M. R.; Varner, M. E.; Stanton, J. F.; Ellison, G. B. Propargyl Radical: Ab Initio Anharmonic Modes and the Polarized Infrared Absorption Spectra of Matrix-Isolated $HCCCH_2$. *J. Phys. Chem. A* **2005**, *109*, 3812–3821.

Bibliography

Four members of the ROT&Comp lab (Department of Chemistry "Giacomo Ciamician", University of Bologna). From left to right: *Cristina Puzzarini* is professor of Physical Chemistry at the University of Bologna and head of the ROT&Comp lab at the Department of Chemistry "Giacomo Ciamician". Her research activity spans from computational chemistry and spectroscopy to experimental rotational spectroscopy. Her main research interest is astrochemistry, with special focus on spectroscopic and computational studies in support of astronomical observations and investigation of interstellar chemistry. *Luca Bizzocchi* earned his PhD in Chemistry at University of Bologna in 2002; he has been post-doctoral fellow in Bologna, Lisbon, and at the Max-Planck Institute for Extraterrestrial physics, Garching. Since 2021, he has a tenure-track professorship at the Department of Chemistry "Giacomo Ciamician". His interests are molecular physics and astrochemistry, with a particular focus on high-resolution molecular spectroscopy and millimeter-wave astronomy. *Silvia Alessandrini* received her PhD cum laude in May 2022 at Scuola Normale Superiore (Pisa). Currently, she is a postdoctoral fellow at the Department of Chemistry "Giacomo Ciamician". Her interest involves computational studies related to rotational and ro-vibrational spectroscopy, development and validation of accurate computational protocols to be employed in spectroscopic studies and modeling of gas-phase chemistry in astrochemical and combustion processes. *Mattia Melosso* got his PhD in Chemistry at University of Bologna in 2020. Currently, he is

Junior Assistant Professor of Physical Chemistry at the Department of Chemistry "Giacomo Ciamician". His research interests are rotational and ro-vibrational spectroscopy, and the discovery of new interstellar molecules.

Vincenzo Barone has been professor of Physical Chemistry at the Federico II University of Naples since 1994 and professor of Theoretical and Computational Chemistry at the Scuola Normale Superiore (SNS) in Pisa since 2008. After his retirement in November 2023, he has been continuing his research activity at the Italian National consortium for the Science and Technology of Materials (INSTM), also supported by a R&D grant from Gaussian Inc. His research activity is witnessed by about 900 papers in international journals with an H-index of 100 and more than 60000 citations. He also covered several management positions, including the presidency of the Italian Chemistry Society and the Direction of SNS. His main research interests include computational thermochemistry, kinetics and spectroscopy, development of density functionals and solvent models, and –more recently– the use of machine learning and virtual reality in several fields of molecular sciences.

TOC Graphic

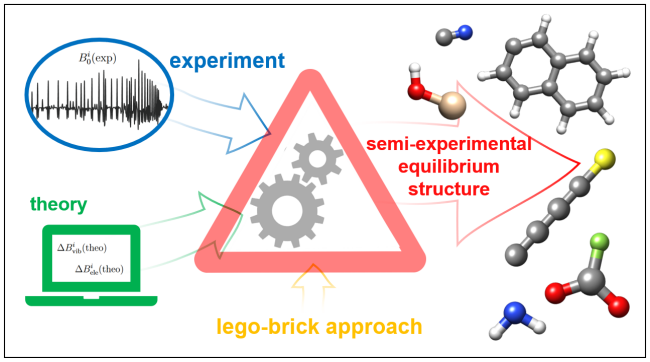
B_0^i(exp)
experiment
theory
ΔB_{vib}^i(theo)
ΔB_{ele}^i(theo)
semi-experimental
equilibrium
structure
lego-brick approach